

Investigating Strategies for Mitigating Iodine-Induced  
Stress Corrosion Cracking in CANDU® Fuel Sheathings

Enquête de Stratégies pour Atténuer la Fissuration par  
Corrosion Sous Contrainte par Induite par l'Iode dans les  
Gaines de Combustible CANDU®

A Thesis Submitted to the Division of Graduate Studies of the Royal Military  
College of Canada by

Joseph Francis Metzler

In Partial Fulfillment of the Requirements for the Degree of Master of Applied  
Science

November 2018

© This thesis may be used within the Department of National Defence but  
copyright for open publication remains the property of the author.

To Rach, Roman, and everyone else that helped me through this process.

## Acknowledgements

Thank you to everyone at the RMC that assisted in the experiments and research that went into this work. I have learned much and appreciate all the guidance I have received. Special thanks to Dr. Corcoran for all the support and patience throughout the process.

## Co-Authorship Statement

This thesis was completed as part of a research program at RMC. See Section 1.9.1 for a detailed explanation of the contribution of the author of this thesis to said program.

## Abstract

CANDU<sup>®</sup> fuel uses the graphite-based coating CANLUB to mitigate iodine-induced stress corrosion cracking (I-SCC) and has an excellent record of fuel performance with very low failure rates ( $\approx 0.01\%$ ). Advanced fuelling cycles should be considered (*e.g.*, higher burnups or power cycling) to increase efficiency and cost effectiveness in reactors. With a corresponding increase in fission product inventory and load cycling, strategies on improved I-SCC mitigation are necessary to facilitate the move to a more aggressive fuelling schedule.

Building upon previous research at the Royal Military College of Canada, this thesis will aim to investigate alternative methods for mitigating I-SCC. This will involve utilizing established static loading methods to test the viability of small oxygen additions using O<sub>2</sub> gas and alkaline oxide additions (*e.g.*, Na<sub>2</sub>O and CaO).

This thesis will discuss the relevant background on CANDU fuel, I-SCC, and the motivation for investigating advanced fuel cycles. The experimental apparatuses and procedures will also be discussed.

Results from static loading tests have shown that O<sub>2</sub> gas additions have a small effect with respect to reducing the amount of corrosive attack experienced on Zircaloy-4. CaO and Na<sub>2</sub>O have shown the ability to reduce the amount of corrosive attack experienced on Zircaloy-4. Also, results are presented from an experiment that showed an alternative commercially available coating, Pyromark, has higher levels of impurities (*e.g.*, Ca and Na) and offers increased I-SCC mitigation potential over that of traditional CANLUB.

## Résumé

La combustible CANDU® utilise un matériau de recouvrement à base de graphite CANLUB pour atténuer la fissuration par corrosion sous contrainte induite par l'iode (FCC-I) et a une compte rendu excellente de performance combustible avec des taux de faillites très bas ( $\approx 0.01\%$ ). Des cycles de ravitaillement élevées devrais être considérés (ex. plus de combustions ou cycles de puissance) pour améliorer l'efficacité et rentabilité dans les réacteurs. Avec un correspondant accroissement de produits de fission et cycle de charge, des stratégies sur l'amélioration d'atténuation de FCC-I est nécessaire pour faciliter le changement vers un programme de ravitaillement plus agressif.

S'appuyant sur des recherches précédentes menées au Collège militaire royal du Canada, cette thèse se vise à enquêter de méthodes alternatives d'atténuation de FCC-I. Cela impliquera l'utilisation de méthodes de chargement statique établis pour tester la viabilité de peu d'additions d'oxygène utilisant le gaz  $O_2$  et additions d'oxydes alcalins (ex.  $Na_2O$  et  $CaO$ ).

Cette thèse discutera le contexte pertinent sur la combustible CANDU®, FCC-I, et la motivation pour enquêter des cycles de ravitaillement avancées. Les appareils et procédures expérimentaux seront aussi discutés.

Les résultats des tests de chargement statique ont montré que les additions de gaz  $O_2$  ont un petit effet en ce qui concerne la réduction de la quantité d'attaque corrosive qu'expérience le Zircaloy-4.  $CaO$  et  $Na_2O$  ont démontrés la capacité à réduire le montant d'attaque corrosive qu'expérience les échantillons de Zircaloy-4. Aussi, les résultats sont présentés à partir d'une expérience qui a montrer un recouvrement alternatif disponible dans le commerce, Pyromark, a des niveaux d'impuretés plus élevés (ex. Ca et Na) et offres le potentiel d'atténuation augmenté pour FCC-I au-delà du traditionnel CANLUB.

## Table of Contents

<b>Table of Figures</b> .....	<b>viii</b>
<b>Table of Tables</b> .....	<b>x</b>
<b>List of Acronyms</b> .....	<b>xii</b>
<b>List of Symbols</b> .....	<b>xiii</b>
1 Introduction.....	1
1.1 Canadian Nuclear Reactors for Power Generation.....	1
1.1.1 CANDU Reactor Technology .....	2
1.2 CANDU Reactor Fuel .....	4
1.3 Fission Product Inventory of Iodine .....	6
1.4 Zircaloy in CANDU Reactors .....	7
1.4.1 Zircaloy-2 and Zircaloy-4.....	7
1.5 Iodine-induced Stress Corrosion Cracking from Pellet-Cladding Interaction	8
1.5.1 Strain Levels in CANDU Fuel Sheathing.....	8
1.5.1.1 Oxide Layer Formation and Cracking .....	10
1.5.2 Mechanism of Iodine-induced Stress Corrosion Cracking .....	10
1.6 Stress Corrosion Cracking Mitigation Strategies in CANDU Reactors .....	11
1.6.1 CANLUB Coating.....	12
1.6.2 Influence of Initial I-SCC Mitigation Strategies on Fuel Failure Rates .....	13
1.7 Motivation for Investigating Alternative SCC Mitigation Strategies .....	13
1.8 Nuclear Power and the Electricity Market of Ontario .....	14
1.8.1 Electrical Energy Production in Ontario.....	14
1.8.2 Nuclear Power Industry of Ontario.....	15
1.8.2.1 Electricity Market of Ontario.....	15
1.8.3 The Future of Energy Production in Ontario .....	18
1.8.4 Increasing Power Outputs in Current CANDU Units.....	19
1.8.5 Increasing the flexibility of CANDU units.....	19
1.9 Investigating Alternative Stress Corrosion Cracking Mitigation Strategies.	20

1.9.1 RMC I-SCC Mitigation Research Program .....	20
1.10 Slotted Ring Experiment .....	22
1.10.1 Static Loading .....	22
1.10.2 Alkaline oxide additives in CANLUB .....	23
1.10.3 Inclusion of Oxygen .....	23
2 Goals of Research .....	25
3 Experimental Apparatuses and Procedures .....	26
3.1 Experimental Matrix Design .....	26
3.2 Slotted Ring Preparation .....	27
3.3 Static Loading .....	28
3.3.1 O <sub>2</sub> Additions .....	31
3.3.2 Dopant Additions .....	32
3.4 Deflection Measurements .....	32
4 Results and Analysis .....	35
4.1 Static Loading Results .....	35
4.2 Analysis of Baseline Slotted Rings .....	36
4.2.1 I-SCC Static Loading Results .....	37
4.2.1.1 I-SCC Static Loading Deflection Measurements .....	38
4.2.1.2 I-SCC Static Loading Slot Size Measurements .....	42
4.3 Oxygen Additive Static Loading Results .....	43
4.3.1 Oxygen Additive Static Loading Deflection Measurements .....	44
4.3.1.2 Oxygen Additive Static Loading Slot Size Measurements .....	47
4.4 Alkaline Metal Oxide and Alkali Earth Metal Oxide Additive Static Loading Results 48	
4.4.1 Alkaline Metal Oxide and Alkali Earth Metal Oxide Additive Static Loading Deflection Measurements .....	48
4.4.2 Alkaline Metal Oxide and Alkali Earth Metal Oxide Additive Static Loading Slot Size Measurements .....	51
4.5 Protective Coating Static Loading Results .....	51

5	Discussion.....	54
5.1	I-SCC Bare Ring Experiments .....	54
5.2	Comparison with previous work investigating O <sub>2</sub> Additions .....	54
5.3	Feasibility of Metal Oxide Additives .....	55
5.4	Coatings.....	57
5.5	Potential Effects of Radiation on Metal Oxide Additives .....	58
6	Conclusions.....	61
7	Future Recommendations .....	63
7.1	Further Investigation into O <sub>2</sub> Gas Additions .....	63
7.2	Further Investigation into Oxide Additives .....	63
7.3	Further Pyromark Testing.....	64
7.4	Irradiation Testing .....	64
7.5	Advanced Fuel Cycles and Dynamic Loading .....	64
8	References.....	66

## Table of Figures

Figure 1: Fission process caused by the collision of a neutron and the nucleus of an atom. Nuclear reactors utilize the energy released in this process to create electricity. Adapted from [6].....	2
Figure 2: Fission cross-sections of U-235, U-238, and Pu-239. Note that both axes are logarithmic. Adapted from [12]. .....	3
Figure 3: Schematic of a CANDU nuclear power plant (NPP), adapted from [15,16].....	4
Figure 4: Overview of CANDU fuel, adapted from [15].....	5
Figure 5: Cross-section of a CANDU fuel sheathing once placed in service, adapted from [17].....	6
Figure 6: Plot of fuel-sheath gap closure over time at a linear power of $25 \text{ kW m}^{-1}$ [27].....	9
Figure 7: Depiction of stress corrosion cracking process in CANDU reactors. Adapted from [2] .....	11
Figure 8: Zr-4 slotted ring samples and a Zr-4 static wedge. ....	28
Figure 9: Loaded slotted ring samples. ....	29
Figure 10: Glass vial containing iodine. ....	29
Figure 11: Necked down glass ampoule. ....	30
Figure 12: Vacuum system for evacuating ampoules. ....	30
Figure 13: Sealed ampoule with iodine capsule inside furnace before heating. ....	31
Figure 14: The purple glow of iodine vapour. ....	31
Figure 15A: First valve configuration. $\text{O}_2$ gas is flushing air out of system up to three-way valve. The vacuum pump is removing air up to the three-way valve, including both bleed valves. B: Second valve configuration. $\text{O}_2$ gas is now free to flow through the consecutive bleed valves. ....	32

Figure 16: SEM images of (A) a Zr-4 ring surface after being exposed to 300 °C on a 9 mm wide wedge and (B) A Zr-4 ring surface after being exposed to the same condition as (A), except 1530 mg of I <sub>2</sub> were introduced to the experiment. ....	33
Figure 17: Apparatus for performing deflection measurements, adapted from [54]. .....	34
Figure 18: Average deflection results at 300 °C of ring samples on 9 mm wedges vs. iodine. ....	40
Figure 19: Average deflection results for all samples tested without iodine vs. temperature. ....	40
Figure 20: Average deflection results for experiments performed vs. wedge size. 41	
Figure 21: 95 g deflection results for all O <sub>2</sub> gas tests. Red squares denote outliers and orange circles display the average deflection at each O <sub>2</sub> level (excluding outliers). The trend line and R <sup>2</sup> value are based on average deflection values for each O <sub>2</sub> gas level. ....	45
Figure 22: Average Na <sub>2</sub> O deflection results (error bars = 1 σ). ....	50
Figure 23: Average CaO deflection results (error bars = 1 σ). ....	50
Figure 24: Relationship between I <sub>2</sub> production and burnup, adapted from Table 2. .....	57

## Table of Tables

Table 1: Neutron absorption cross-sections for thermal (0.0253 eV) and fast (14 MeV) neutrons [].

Table 2: Summary of iodine concentrations at varying burnups, adapted from [10].

Table 3: Elemental composition of Zr-2 and Zr-4 (minor impurities are not shown). [24].

Table 4: Concentrations of Na, Ca, and Mg present in CANLUB, adapted from [38]

Table 5: Energy production for Ontario in 2017 by technology [].

Table 6: Percentage of electricity supplied by energy generation technologies in Ontario [].

Table 7: 2016 LUEC estimates from the IESO for the different energy production technologies within Ontario [].

Table 8: Static loading experimental matrix. Where N is the number of replicates.

Table 9: Average deflections and slot sizes for three distinct batches of slotted ring samples solely subjected to the cutting process. Each batch contained 3 samples. Numbers in bold express the average deflections and slot size for all nine rings tested. The error attached to each value is one standard deviation.

Table 10: Associated *p-values* from ANOVA analyses of baseline batches of slotted rings.

Table 11: Summary of I-SCC static loading conditions (N = number of samples).

Table 12: Preliminary regression results from I-SCC deflection results.

Table 13: Updated regression results from I-SCC deflection results.

Table 14: Regression results from I-SCC slot size results.

Table 15: Test conditions for investigation into effects of O<sub>2</sub> gas on I-SCC.

Table 16: Preliminary oxygen gas regression results.

Table 17: Regression results on final slot sizes for I-SCC tests including O<sub>2</sub> gas.

Table 18: Summary of the experimental conditions for investigating the influence of metal oxides on I-SCC of Zr-4 rings.

Table 19: Initial regression results for metal oxide additive experiments.

Table 20: Final regression statistics on deflection results where moles of metal oxides are the inputs.

Table 21: Results from regression analysis on the effect of CaO and Na<sub>2</sub>O on the final slot size of Zr-4 rings that have undergone I-SCC experiments.

Table 22: 45 g deflections for uncoated, CANLUB coated, and Pyromark coated rings; adapted from [59].

Table 23: 95 g deflections for uncoated, doped CANLUB coated; adapted from [59].

Table 24: Notable products of neutron activation of 0.01 gCa exposed to flux levels of CANDU reactors for 1 year,

Table 25: Notable products of neutron activation of 0.04 gNa exposed to flux levels of CANDU reactors for 1 year, adapted from calculations by [71].

## Table of Acronyms

I-SCC – Iodine-Induced Stress Corrosion Cracking

Zr-4 – Zircaloy-4

CANDU® – CANada Deuterium Uranium

PHT – Primary Heat Transport

Zr-2 – Zircaloy-2

PCI – Pellet Cladding Interaction

IESO – Independent Electricity Supplier of Ontario

BNGS – Bruce Nuclear Generating Station

DNGS – Darlington Nuclear Generating Station

PNGS – Pickering Nuclear Generating Station

OPG – Ontario Power Generation

OEB – Ontario Energy Board

NPP – Nuclear Power Plants

LUEC – Levelized Unit Electricity Cost

IAEA – International Atomic Energy Agency

LTEP – Long Term Energy Plan

ICPMS – Inductively Coupled Plasma Mass Spectrometry

ANOVA – Analysis of Variances

## List of Symbols

$D_y$  - Expected deflection

$F_y$  - Weight force

$l$  - Width of the ring

$t$  - Thickness of ring

$R$  - Radius of ring

$E$  - Young's Modulus

$\sigma_A$  - Maximum analytical tensile stress

$w$  - Final slot position

$w_0$  - Initial slot opening

$\alpha$  - Half of the angle of the slot in degrees

# 1 Introduction

This thesis will investigate the process of iodine-induced stress corrosion cracking (I-SCC) in Zircaloy-4 (Zr-4) alloy fuel sheathing used in CANDU® (CANada Deuterium Uranium) reactors. I-SCC is a dynamic process that can occur when CANDU fuel pellets expand and interact with the surrounding sheathing in the presence of corrosive fission products (*e.g.*, iodine), causing failures in the sheath. Sheath failures are undesirable as they can allow highly radioactive fission products into the Primary Heat Transport (PHT) system, which is a system that uses heavy water to remove heat from the fuel and transports this heat to the steam generators to produce electrical power *via* the steam cycle. There are numerous risks associated with elevated radiation fields in the plants, with personnel safety first among them. Beyond safety concerns, sheath failures would necessitate costly unplanned outages and maintenance for reactor units.

In this thesis, the I-SCC phenomenon was investigated *via* a series of tests on Zr-4 slotted ring samples using static loading procedures. The method utilised was adapted from Wood [1] whereby static loads were applied to slotted rings using static wedges.

This work investigates a potential I-SCC mitigation strategy first proposed by Lewis *et al.*, [2] that involves introducing controlled amounts of alkali metal oxide impurities to the coating applied to the sheath during fuel manufacturing process. This investigation was expanded to include alkaline earth metal oxides as they have a similar molecular structure and thus may have similar I-SCC mitigation abilities.

This chapter sets the context for this thesis, with a background on the I-SCC phenomenon that is provided after an explanation of CANDU technology. This is followed with an explanation of: (i) the status of nuclear power in Ontario, (ii) its place in the larger electricity market of the province, and (iii) the future of the nuclear industry within the province with respect to electrical power generation. From this, the motivation for the research is derived (*i.e.*, the goals of the research).

## 1.1 Canadian Nuclear Reactors for Power Generation

All the nuclear power reactors currently operating in Canada are of the CANDU design. This sub-section discusses the technology to provide an overview of the design and operation of these units. While there have been minor changes made to the design of the plants over time, the base design for the removal of heat from the fuel, the PHT system, remains essentially the same. As the fuel and the PHT system are the focus of this thesis, a single explanation of the system is sufficient for all current generations of CANDU reactors.

### 1.1.1 CANDU Reactor Technology

CANDU reactors are powered by nuclear fission, the process wherein the nucleus of an atom is split into lighter parts (*i.e.*, fission products) [3]. If a material has the ability to undergo fission, it is said to be fissile. U-235 is a naturally occurring isotope of uranium that is fissile and releases approximately 200 MeV of energy when it undergoes fission. This energy is converted into electrical energy by the secondary side of the unit wherein the steam created by the thermal energy of fission is sent through a turbine-generator set [4].

When fission occurs, there is also a simultaneous release of two to three neutrons [5]. Figure 1 displays a general case of the fission process initiated from the absorption of a neutron with a fissile nucleus.

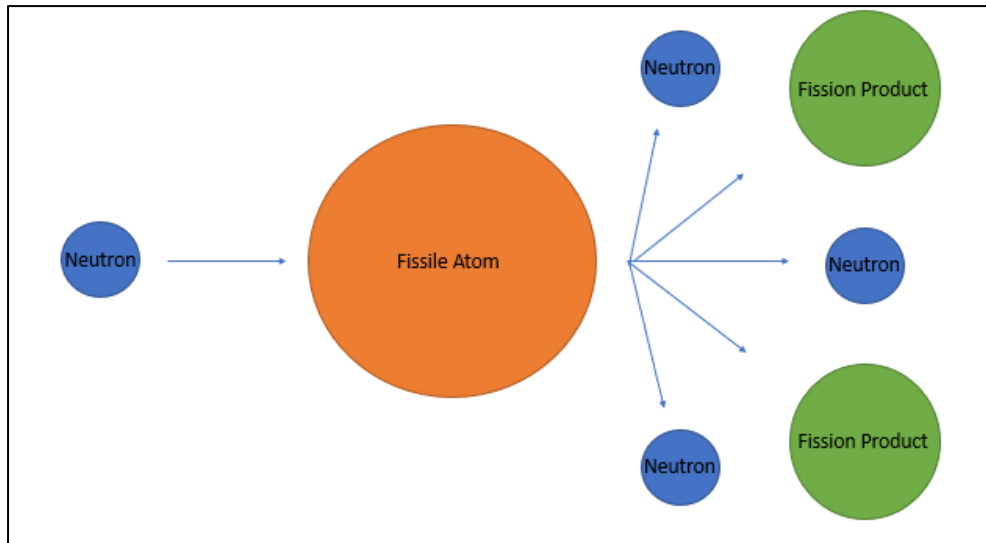


**Figure 1: Fission process caused by the absorption of a neutron and the nucleus of a fissile atom. Nuclear reactors utilize the energy released in this process to create electricity *via* the steam cycle. Adapted from [6].**

The neutrons released by the fission process are fast neutrons (*e.g.*, kinetic energy range of 1-20 MeV [7]), which when moderated or thermalized (*e.g.*, kinetic energy at or below 0.025 eV [8]) are more likely to cause further fissions in other fissile isotopes. Not all fission neutrons produced go on to cause subsequent fissions, as some are lost to leakage or absorption during the moderation process. However, to maintain a reactor's criticality (*e.g.*, the number of fissions in one generation equal to the number of fissions in the next generation) [9], at least one neutron for a given fission interaction must go on to cause a subsequent fission.

Not all neutron absorption in a CANDU reactor is parasitic. For example, CANDU reactors are fuelled by natural uranium dioxide fuel. Natural uranium mainly consists of the isotope U-238 (99.3% by weight) and U-235 (0.7% by weight) [10]. U-235 is a fissile isotope, while U-238 is a fertile isotope that will capture neutrons and undergo a series of beta-minus decays to become the fissile isotope Pu-239 [11].

Figure 2 displays the neutron cross-sections for fission corresponding to the main isotopes in CANDU reactors. A neutron cross-section expresses the likelihood of a specific interaction occurring between an isotope and a neutron of a specific energy level. Thus, this chart displays the likelihood of fission occurring within U-235, U-238, and Pu-239 when interacting with a free neutron as a function of neutron energy.

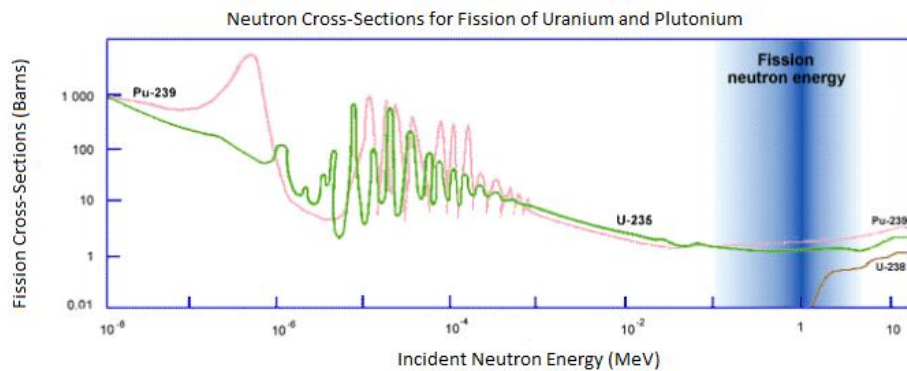


**Figure 2: Fission cross-sections of U-235, U-238, and Pu-239. Note that both axes are logarithmic. Adapted from [12].**

Table 1 lists the cross-sections for absorption with U-235, U-238, and Pu-239 for both fast and thermal neutrons.

**Table 1: Neutron absorption cross-sections for thermal (0.0253 eV) and fast (14 MeV) neutrons [13]**

Isotope	Neutron absorption cross-section / barn	
	$\leq 0.0253$ eV	14 MeV
U-235	98.7	$889.7 \times 10^{-6}$
U-238	2.7	$589.4 \times 10^{-6}$
Pu-239	271.5	$847.4 \times 10^{-6}$

The desired interaction for U-235 and Pu-239 is fission, and for U-238 the desired reaction is capture. It can be seen from Table 1 and/or Figure 2 that the neutron absorption for each isotope occurs at a higher frequency when thermal neutrons are

present, as opposed to fast neutrons. CANDU reactors use a heavy water ( $D_2O = {}^2H_2O$ ) moderator to slow fast fission neutrons (*via* scattering interactions) into the thermal neutron energy range and thereby increase the likelihood of neutron absorption, which results in fission and capture interactions.

CANDU reactors operate using horizontal fuel bundles of sintered natural uranium dioxide ( $UO_2$ ) fuel pellets that are encased in Zircaloy-4 (Zr-4) that are moderated and cooled using  $D_2O$  [14]. Figure 3 depicts the main reactor function between the fuel and the steam generator. The heavy water coolant is contained within pressure tubes at a pressure of approximately 10 MPa and is cycled past the fuel to the steam generator [15]. The heavy water moderator is contained within the calandria (the vessel containing moderator (heavy water) in Figure 3) at a lower pressure and temperature than the completely separate PHT system. Neutron economy requires consideration when selecting material within the reactor, including in the design of the fuel.

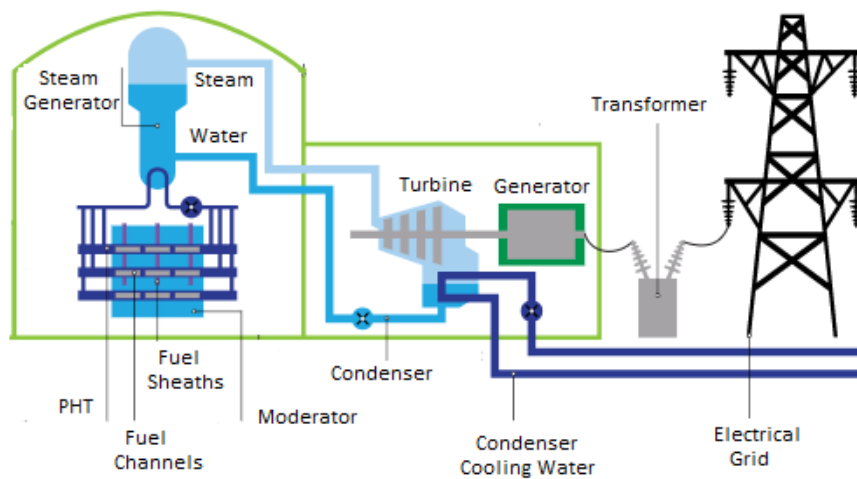


**Figure 3: Schematic of a CANDU nuclear power plant (NPP), adapted from [16,17].**

As this thesis focuses on the fuel and its surrounding components in CANDU reactors, Section 1.2 provides a detailed explanation of CANDU reactor fuel.

## 1.2 CANDU Reactor Fuel

The first components of CANDU reactor fuel are the sintered uranium dioxide ( $UO_2$ ) pellets [18]. The pellets are assembled into fuel sheaths and are enclosed with two welded endcaps to create a fuel element [18]. The inner surface of the sheathing has a protective coating called CANLUB [19]. The CANLUB is a primary focus of this thesis as it is used for I-SCC mitigation in operating reactors, and as such, it is discussed in detail in Section 1.6.1. Fuel elements are then collected into fuel bundles with 20-40 fuel elements, also referred to as elements, where each element contains

20-40 fuel pellets [18]. Bundles are loaded into the horizontal fuel channels. Figure 4 depicts the hierarchy of CANDU fuel.

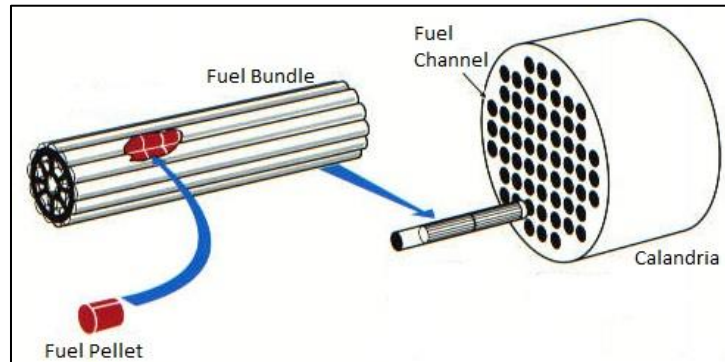


**Figure 4: Overview of CANDU fuel, adapted from [16].**

The pellets are smaller diametrically than the sheathing, leaving a gap of about 100  $\mu\text{m}$  between the fuel and sheath [20]. The gap allows for fission gas release and provides space to allow for the thermal expansion of the pellets. Another feature of CANDU fuel pellets that allows for thermal expansion is the geometry of the pellets themselves. The pellets are slightly narrower in the centre region, creating an hourglass shape, and there is a dish set into the top and bottom of the pellet [21]. This creates space for the pellets as they swell. Using an irregular pellet at the end of the fuel element creates a space between the end of the pellets and the endplates to allow for axial thermal expansion of the pellets. The pressurized PHT coolant flows over the fuel at a pressure of approximately 10 MPa [15]. The pressurized coolant causes the sheath to collapse around the fuel pellets.

Figure 5 is a depiction of a cross-section of a CANDU fuel element that has been placed into service and is displaying all these features. Note the circumferential ridges on the sheath, which causes a wavy appearance and contributes to the stress profile in the sheath [18]. Sheath stress is discussed further in Section 1.5.1.

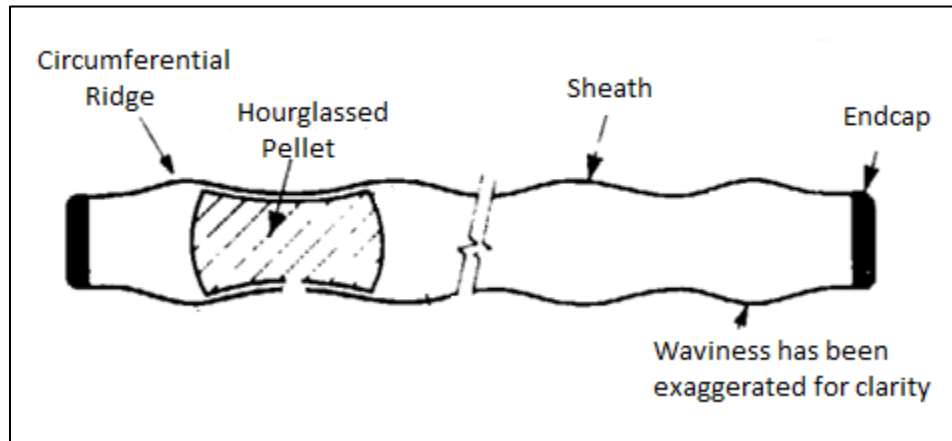


Figure 5: Cross-section of a CANDU fuel sheathing once placed in service, adapted from [18].

Zr-4 was selected for the sheath material because of its mechanical and neutronic properties, which are detailed in Section 1.4. The sheathing is important because it provides fission product containment as well as protection against fuel oxidation.

The research described in this thesis focuses on the interaction of the fuel with the sheath in the presence of corrosive fission products. The following section provides details of the fission product inventory, in terms of iodine. It should be noted that both the fission products iodine and caesium are of interest because of their corrosive effects on the sheath materials. However, as discussed in Section 1.5.2, iodine is the focus of this thesis whereas caesium was not investigated because the radiolysis required to dissociate CsI would have made the experiments prohibitively costly and significantly more hazardous. After fission product inventory is discussed, a summary of the characteristics of the material Zircaloy is provided.

### 1.3 Fission Product Inventory of Iodine

The main element in CANDU fission gas release that is investigated for its corrosive properties in this research is iodine in the form of  $I_2$ . Table 2 outlines the weight fractions of  $I_2$  over a series of burnups, with the fission product mass as the numerator and the initial mass of U as the denominator, according to calculations performed by Clegg and Coady using the computer code CANIGEN [10]. The term burnup is used as a measure of the amount of energy produced per mass of material fissioned. For example, the average burnup in CANDU reactors is  $7-9 \text{ GWd}\cdot\text{t(U)}^{-1}$ .

**Table 2: Summary of iodine concentrations at varying burnups, adapted from [10]**

<b>Burnup / MWh kgU<sup>-1</sup> ± 1%</b>	<b>Iodine / mg kg<sup>-1</sup> Initial Uranium ± 10%</b>
39	9.49
139	38.6
180	51.8
222	65.4
319	93.9

As can be seen in Table 2, the amount of iodine produced increases with burnup. The following subsections will provide specifics on Zircaloy.

#### **1.4 Zircaloy in CANDU Reactors**

Zirconium-based alloys known as Zircaloy are used in the nuclear industry due to their low neutron absorption cross-section, strong mechanical properties, and excellent corrosion resistance. In CANDU reactors Zircaloy alloys are used for fuel sheathing, structural materials, and pressure tubes.

##### **1.4.1 Zircaloy-2 and Zircaloy-4**

The two main Zircaloy alloys used in most nuclear reactors are Zircaloy-2 (Zr-2) and Zircaloy-4 (Zr-4). In CANDU reactors, Zr-4 is the fuel sheathing material and Zr-2 is the pressure tube material [22]. Zr-4 was developed from Zr-2 with the desire to reduce the tendency to absorb hydrogen by removing the nickel content and by limiting the range of iron weight content [23]. This is shown in Table 3, where the alloy components listed were included for their strengthening effects as well as an attempt to neutralize the effects that impurities may have on corrosion resistance capabilities [24].

**Table 3: Elemental composition of Zr-2 and Zr-4 (minor impurities are not shown). [24].**

<b>Zirconium Alloys</b>	<b>Sn / wt%</b>	<b>Fe / wt%</b>	<b>Cr / wt%</b>	<b>Ni / wt%</b>	<b>Zr / wt%</b>
Zr-2	1.2-1.7	0.07-0.20	0.05-0.15	0.03-0.08	Balance
Zr-4	1.2-1.7	0.12-0.18	0.05-0.15	0.03-0.07	Balance

The experiments in this thesis are performed on samples of Zr-4, as Zr-4 is the material of CANDU fuel sheathing. The following subsection provides a detailed explanation of I-SCC interactions with Zr from Pellet-Cladding Interactions (PCI).

### **1.5 Iodine-induced Stress Corrosion Cracking from Pellet-Cladding Interaction**

Stress corrosion cracking is a dynamic process of cracking in a metal due to the combined effects of a corrosive environment and straining of the metal. For stress corrosion cracking to occur there are three conditions that must be met [25]:

- A corrosive environment,
- A susceptible material, and
- A critical level of tensile stress to initiate the process.

Zircaloy is susceptible to SCC when under stress and exposed to an iodine vapour at temperatures around or above 300 °C [1]. CANDU fuel reaches a temperature of over 300 °C in the gap between the fuel and the fuel sheathing [26], establishing a high enough temperature to make SCC possible in the sheath, as per the work of Cox [1]. This temperature is also high enough that iodine will be in the vapour phase, meeting the remaining criterion for I-SCC. The next subsections provides further details on I-SCC.

#### **1.5.1 Strain Levels in CANDU Fuel Sheathing**

I-SCC induced cracking is a process that can occur from pellet-sheathing interactions between UO<sub>2</sub> fuel pellets and Zircaloy that surrounds the fuel [27].

The stress fields experienced by the Zircaloy sheathing in CANDU reactors are dependent upon the gap observed between the fuel pellets and the inner radius of the sheath.

Figure 6 plots the radii of both the fuel and the inner surface of the sheath over time at a set linear power, which is the power produced per a set unit length [27]. In the plot, (i) corresponds to the elastic contraction of the sheath, (ii) is the thermal expansion of the sheath, (iii) represents the thermal expansion of the fuel, (iv) displays the creep down of the sheath, and (v) is the initial Pellet Cladding Interaction (PCI). The gap between the sheath and the fuel at (v) is approximately 1  $\mu\text{m}$ . This gap includes a thin oxide layer of  $\text{ZrO}_2$  (ranging from 0.20-0.61  $\mu\text{m}$  [28]) that forms during fabrication on the Zr-4 surfaces; the formation and cracking of this layer is explained further in the following subsection.

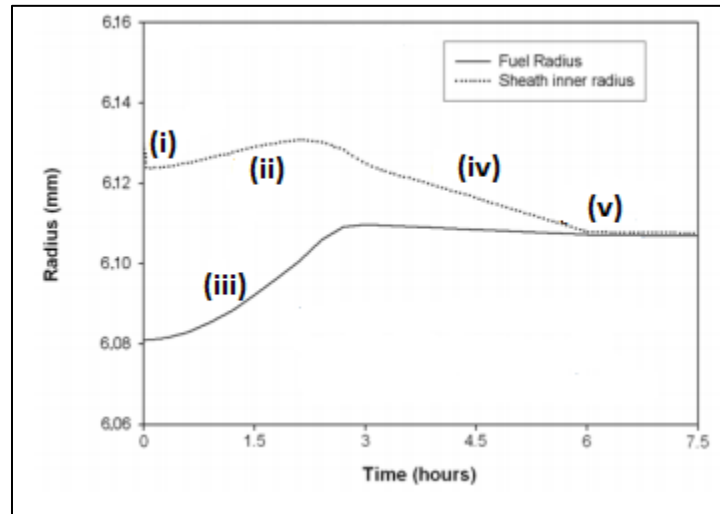


**Figure 6:** Plot of fuel-sheath gap closure over time at a linear power of 25  $\text{kW m}^{-1}$  [28].

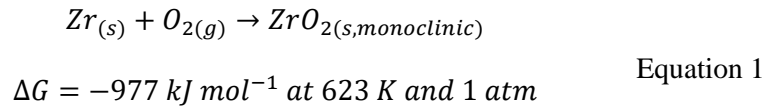
If this  $\text{ZrO}_2$  oxide layer remains intact it will protect the Zr-4 from the corrosive gaseous fission products. To fracture the oxide layer, strain levels between 0.1-0.5% are required [28]. When these strain levels are reached, the oxide layer will begin to form cracks and expose the already hot sheathing to a corrosive environment. Further, it has been predicted that CANDU fuel sheathing can experience hoop strains between 0.8-1.3% during operation [29] (*via* the processes depicted in Figure 6); thus, the critical level of tensile stress to fracture the oxide layer is met by the fuel sheathing within CANDU reactors. Therefore, SCC is possible as the three conditions (*i.e.*, corrosive environment, susceptible material, and a critical level of tensile stress to initiate the process) have all been met.

The cracking of the oxide layer is of considerable importance as it is the first step in the process of I-SCC corrosion. The following section will go into more detail on

the formation and cracking of the oxide layer. The importance of the layer will also be elaborated upon.

#### **1.5.1.1 Oxide Layer Formation and Cracking**

A zirconium oxide ( $ZrO_2$ ) film forms on the surface of Zircaloy when exposed to oxygen. It has been proven that this layer actively protects the Zr-4 from iodine vapour [30]. The tendency for  $ZrO_2$  to form is shown by the chemical reaction displayed below in Equation 1.



The negative Gibb's Free Energy value associated with this reaction indicates that the above reaction is a favoured reaction (*e.g.*, proceeds towards the right). Therefore, for CANDU fuel sheathing, the  $ZrO_2$  oxide layer on the Zr-4 sheathing is stable and will form in the presence of oxygen. Une *et al.*, [30] performed experiments on Zircaloy samples exposed to very high levels of iodine as well as controlled amounts of oxygen and concluded that if a certain amount of oxygen was present the samples will not fail at any iodine concentration. Une *et al.*, work supports the work of Rosenbaum *et al.*, [25,29] stating that if an oxide layer is present, and in tension, cracking will not occur. If there is sufficient stress applied this will cause the oxide layer to crack, exposing the bare metal surface. This can lead to cracking and corrosion of the underlying material. However, it is also believed that a small partial pressure of oxygen may repair some of the cracks in the oxide layer, which would assist in I-SCC prevention [2]. The following subsection will provide an explanation of the I-SCC process as it occurs in CANDU fuel sheathing.

#### **1.5.2 Mechanism of Iodine-Induced Stress Corrosion Cracking**

I-SCC in CANDU fuel sheathing begins when gaseous fission products diffuse through the fuel matrix towards the fuel sheath in areas where the oxide layer has cracked, leaving the metal sheath exposed. As the fission products reach the metal sheath, the corrosive products will begin to form a deposit in the form of CsI. This compound will decompose due to the high levels of radiation present, a process known as radiolysis, and release iodine vapour into the gap [28].

The iodine vapour now in the gap diffuses towards cracks in the oxide layer and interacts with the exposed Zircaloy. The interaction between solid Zr and  $I_2$  vapour produces the gaseous  $ZrI_4$ .  $ZrI_4$  dissociates in the fuel-to-sheath gap releasing iodine

and zirconium back into the environment [2]. This effectively removes zirconium from the sheath while the dissociated iodine is free once more to interact with zirconium in the sheath. This is known as the Van Arkel [2] process and can cause a crack to propagate through the sheath. Figure 7 depicts the I-SCC phenomenon that can occur within the fuel sheath.

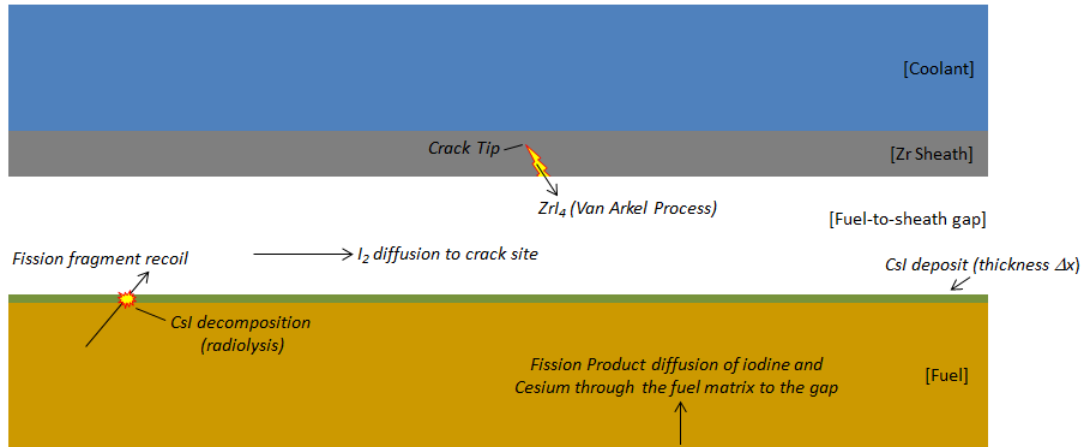


Figure 7: Depiction of stress corrosion cracking process in CANDU reactors. Adapted from [2].

Historically, environmentally assisted cracking, such as I-SCC, accounted for approximately 35% of fuel bundle failures in CANDU reactors [31]. Garzarolli *et al.*, stated that PCI failures could become a larger issue in CANDU reactors if not investigated further [32]. However, 67% of the first 114 confirmed failures in CANDU operation occurred prior to 1973 [33], which is evidence of improved performance since the implementation of the initial I-SCC mitigation strategies. The following section outlines the status of I-SCC mitigation strategies in CANDU reactors that were developed from these initial I-SCC investigations.

## 1.6 Stress Corrosion Cracking Mitigation Strategies in CANDU Reactors

The rate of fuel failures in early operation CANDU reactors was high enough that it led to significant investigative efforts from the industry to determine the cause of these failures. When it was determined by Wood *et al.*, [1] that I-SCC was the most probable cause of these failures, a series of I-SCC specific failure mitigation strategies were explored.

During the initial investigation, it was found that the largest factor in whether fuel failed is whether it underwent large increases in power over a short period of time.

Considering this, a fuel management schedule reduced PCI induced failure rates significantly by reducing the peak power level of the outer fuel elements from 60 kW m<sup>-1</sup> to 53 kW m<sup>-1</sup> [34] and by avoiding the power ramps that led to the previous defects [26].

Also, tests showed that placing a thin (3-20 µm) graphite layer on the inner surface of the sheath led to very low failure rates [35]. These results led to a similar coating entitled CANLUB - *named as such due to the belief that the coating was working as a mechanical lubricant* - being a standard addition in CANDU reactor fuel.

### 1.6.1 CANLUB Coating

Although the coating was originally designed and believed to be a mechanical lubricant and barrier, there are two main reasons why it is believed that CANLUB is not performing these functions:

- 1) The moisture levels experienced in reactor environments do not allow CANLUB to act as a lubricant [36] and
- 2) The porosity of graphite renders it ineffective as a physical barrier [37].

Considering this, it was hypothesized that CANLUB was influencing the chemical composition of the environment within the fuel sheathing. The high temperatures experienced in reactors cause corrosive species, such as I<sub>2</sub> and ZrI, to be collected by volatile carbon to form compounds such as Zr<sub>6</sub>I<sub>12</sub>C. When the corrosive species form these carbon-based compounds, they are no longer able to interact with the Zr-4 surface [2]. Another piece of evidence that points to the suggestion that CANLUB actively collects corrosive species is that when the coating is baked at temperatures higher than 365 °C, Zr-4 sheaths are more susceptible to SCC [37]. This dependency between the baking temperatures of CANLUB and its SCC mitigation abilities is likely due to the decomposition of a specific component of the coating, which also suggests that there are active ingredients collecting corrosive species. Further, an inductively coupled plasma mass spectrometry (ICPMS) analysis was completed (found in Table 4) on a sample of CANLUB wherein there were significant amounts of the impurities with the theorized mitigation potential within the coating – *a result that confirms the presence of the impurities in the coating* [38].

**Table 4: Concentrations of Na, Ca, and Mg present in CANLUB, adapted from [38]**

<b>Impurity</b>	<b>CANLUB / ppm</b>
Na	220 ± 10
Ca	210 ± 30
Mg	18 ± 9

### **1.6.2 Influence of Initial I-SCC Mitigation Strategies on Fuel Failure Rates**

In 1979, of the 150,000 fuel bundles irradiated in CANDU reactors, 0.18% of the bundles failed, with power ramping accounting for 84% of those failures [39]. This failure rate was reduced to 0.06% when CANLUB was introduced along with new fuel handling strategies (Section 1.6). From the 1970s until 1992, of the over 900,000 irradiated bundles, less than 0.1% developed defects, with 35% of those defects due to SCC [31]. Between 1994 and 2006, CANDU reactors displayed a bundle defect rate of 0.01% in Canada, showing how effective current SCC mitigation strategies have become at preventing failure in current reactor conditions. However, this information does not provide any insight as to how the current SCC mitigation strategies would perform at higher burnup or with additional power cycling.

## **1.7 Motivation for Investigating Alternative SCC Mitigation Strategies**

With strong fuel performance established after the implementation of I-SCC mitigation strategies, there was little interest paid to I-SCC outside of power transient conditions [40]. One potential application for advanced I-SCC mitigation strategies is in research being performed on advanced fuel cycle capabilities, such as the specifics of how to reduce the effects of I-SCC under advanced fuelling strategies (*e.g.*, higher burnups and power cycling). Although CANDU fuel has performed well with current fuelling strategies, if advanced fuelling strategies are to be employed, it will need to be shown unequivocally that the fuel will continue its strong performance. If a more complete understanding of CANLUB can be developed, the assistance it offers current fuelling strategies could be projected to advanced fuelling strategies. Further, improvements in the coating material could be made to reduce I-SCC or to extend burnup or power cycling capabilities, thus, allowing CANDU reactors to increase power levels at a faster rate and allow the potential to increase the maximum overall power output.

From Tayal *et al.*, CANDU reactors in Canada currently operate at baseline power levels of about 7-9 GWd·t(U)<sup>-1</sup> so fuel bundles do not experience many power transients in their lifetime [33]. As nuclear power has developed into a larger source of electrical power in Canada, there has been increasing interest to develop the power cycling or “load-following” capability of CANDU reactors. This would lead to increased efficiency as the power level of the reactor will attempt to match the amount of power required by the market. For example, in France, where nuclear power produced 74-79% of its electrical power from 2002-2012 [41], NPPs operate with load-following to improve efficiency. The following section provides an overview of the electricity market in Ontario, with focus placed on nuclear power within the province. This sets the larger context of this research, and to further illustrate the benefit that would be provided to the nuclear power industry, specifically within Ontario, by increasing unit flexibility and output.

## **1.8 Nuclear Power and the Electricity Market of Ontario**

This section lays out the current state of the energy production industry in the province of Ontario, with a focus on nuclear power. The share of the electricity market currently held by each method of energy production is provided with a detailed summary of the costs associated with each of the energy production technologies. The context of the electricity market explains the desirability of moving CANDU units to higher power levels with larger power ramps.

### **1.8.1 Electrical Energy Production in Ontario**

The two main methods of electrical energy production in Ontario in 2017 are nuclear power and hydroelectric generation. Table 5 summarizes the Independent Electricity Supplier of Ontario (IESO) year-end data and shows the share of energy production in Ontario for each method of energy production.

**Table 5: Energy production for Ontario in 2017 by technology [42].**

<b>Generation Technology</b>	<b>Energy Produced / TWh</b>	<b>Energy Produced / % of total production</b>
Nuclear	91.7	61
Hydroelectric	35.7	24
Natural Gas	12.7	9
Wind	9.3	6
Solar	0.5	<1
Biomass	0.5	<1

As shown in Table 5, nuclear power is currently providing the majority of the electrical energy production in the province of Ontario.

### **1.8.2 Nuclear Power Industry of Ontario**

Nuclear power in Ontario has developed a history of reliable performance that was long considered adequate for the province’s energy demands. However, the nuclear industry of Ontario is currently undergoing a transition period with the Bruce Nuclear Generating Station (BNGS) and the Darlington Nuclear Generating Station (DNGS) undergoing refurbishment projects, and Pickering Nuclear Generating Station (PNGS) approaching the end of station life (planned for 2024) [43].

There are currently 18 nuclear power reactor units operating in Ontario, all of which are CANDU design reactors [43]. There are six operating units at PNGS, four operating units at DNGS, and eight units at BNGS. All these nuclear units were built by, and are owned by, the Crown Corporation Ontario Power Generation (OPG). All the units are operated by OPG, with the exception of BNGS, which is operated by the private company Bruce Power [44].

#### **1.8.2.1 Electricity Market of Ontario**

There is significant competition in the electrical energy market of Ontario challenging the future of nuclear power. The Province has built a large amount of infrastructure to capitalize on the hydroelectric generation that is possible in the

province. The stability of cheap power provided by ‘hydro’, combined with the strong public opinion from an environmental standpoint, ensures hydroelectric generation will continue to be a large part of Ontario’s energy plan.

Table 6 shows the average cost to consumers for each type of power generation in Ontario, taken from the Ontario Energy Board (OEB) 2017 Price Report [45]. These recent data show that nuclear can be produced in large amounts as 60% of Ontario’s energy production is from nuclear.

**Table 6: Percentage of electricity supplied by energy generation technologies in Ontario [45]**

<b>Generation Technology</b>	<b>% of Total Supply</b>
Nuclear	60
Hydro	24
Gas	6
Wind	8
Solar	2

Table 6 shows that nuclear has the second lowest cost per kilowatt-hour and approximately the third of the price of natural gas. It should be noted that the rates for the cost of power produced by nuclear power follows an agreement made between the Province, through the OEB, and the two companies producing nuclear power. As OPG is a crown corporation, energy prices are set to a level by the Province that ensures the survivability of OPG while attempting to lower the prices for the provincial taxpayers. As such, OPG is paid approximately 40% less than the average price paid to other generators [46]. While the cost for nuclear power in Table 6 is lower than what would be seen in a free market with a private company, the same can be said for the cost of hydro power (the main competitor to nuclear in terms of raw total unit cost) as the hydroelectric generation facilities in Ontario are also operated by OPG [47].

The unit costs in Table 6 do not include the costs associated with constructing and deconstructing the actual power plants themselves, a part of the economics where NPPs tend to fair much worse than the other options due to the size, complexity, and safety requirements associated with nuclear power production.

A more holistic understanding of the cost associated with each type of power generation can be gained through a metric called Levelized Unit Electricity Cost (LUEC). The International Atomic Energy Agency (IAEA) defines LUEC as:

*“A standard technique for comparing different types of power plants with different relative cost components (represents the price of electricity produced, to be charged to recover all costs during operating lifetime of a plant. It includes capital costs, operation and maintenance costs, and fuel costs.)” [48].*

The IESO produced LUEC estimates for the different energy technologies utilized in Ontario; the low and high estimates are shown for each energy production technology (Table 8).

**Table 7: 2016 LUEC estimates from the IESO for the different energy production technologies within Ontario [49].**

<b>Generation Technology</b>	<b>Low LUEC estimate / \$ MWh<sup>-1</sup></b>	<b>High LUEC Estimate / \$ MWh<sup>-1</sup></b>
Nuclear	120	290
Hydro	120	240
Natural Gas	80	310
Wind	65	210
Solar	140	290
Bioenergy	160	260

The most noteworthy observation in this table is the amount of overlap in LUEC values – *there is an overlap of possible LUEC values between 160-210 \$/MWh that features all six energy production methods that is indicative of the inherent uncertainties in these values.* Nevertheless, it is clear, that in terms of LUEC values, nuclear is not capable of presenting itself as an energy production method that is significantly more economic than any others currently in the marketplace. With the lower raw unit costs, evidenced by the low price of nuclear power in Ontario, being offset by the large pre/post-operation costs, shown by LUEC values, nuclear power is not presenting a compelling argument in terms of raw economics, based on the values from Table 7. These observations show it is possible that nuclear power will struggle to be established as the energy production technology of choice moving forward in Ontario without improvements made to the economic performance of current and future reactors. The following subsection elaborates upon this by discussing nuclear power in the context of the future of energy production in Ontario, with suggested potential improvements that could be made to current and future reactors and would improve economic performance.

### **1.8.3 The Future of Energy Production in Ontario**

If the DNGS and BNGS refurbishment projects are executed as planned, there will be two large sources of nuclear energy production servicing the grid for the foreseeable future. OPG claims that DNGS's refurbishment will allow for the station to provide power until 2055 [50]. Bruce Power is planning on its units producing power until 2064 [51]. However, even if the refurbishment projects at DNGS and BNGS are completed successfully, there will still be a requirement for energy production beyond what is provided by these two sites in conjunction with the currently available non-nuclear electric production of the province.

The Long-Term Energy Plan (LTEP) currently predicts there will be a shortfall in generating capacity starting in 2023, after the first two Pickering Units are taken offline and while units are being refurbished at Bruce and Darlington [52]. This problem is further exacerbated when the remaining units are removed from service after 2024 [52]. Currently the LTEP is crediting a redesigned energy market that "*will allow existing and new clean generation facilities to compete in a robust market*"; essentially, the private sector will be looked to in order to bridge the gap between the demand and the supply.

The main way the CANDU units operating in Ontario could make up part of the future shortfall would be by increasing the maximum output of the units. This can be achieved through increasing the maximum power level and/or by increasing the maximum rate that power levels are increased; thus, allowing the units to spend less time at lower power levels. If additional capacity is eventually added, there is a potential for a power surplus as projected in 2019 in the LTEP [52]. Therefore, it would also be desirable to increase the flexibility of unit power regimes, so they can be more responsive to power demands (as opposed to the current base load production regime).

In order to move CANDU units to a more advanced fuelling strategy (*i.e.*, load following, increasing power ramp rates, or increasing overall unit power levels), the nuclear power generation community will need to provide sound evidence that there will be no I-SCC concerns associated with exposing the fuel to any of these strategies. The following subsections will discuss the advanced fuelling strategies with an explanation of the relationship between these strategies and I-SCC mitigation.

#### 1.8.4 Increasing Power Outputs in Current CANDU Units

In order to increase power levels in CANDU units, one must first understand how the changes would manifest in relation to the fuel. It has been shown that increased power levels lead to increased cladding stresses due to fission product swelling in the fuel [53]. In addition, fuel also experiences increased internal gas pressure and increased radiation levels [53]. The total inventory of fission products also increases (discussed in Section 1.3). Thus, high power production levels contributes to higher stresses in the sheath and/or increased levels of fission product inventory.

Current I-SCC mitigation strategies in Ontario CANDU units have been shown to be less effective when burnups reach  $20 \text{ GWd}\cdot\text{t(U)}^{-1}$ ) and the amount of CANLUB remaining on the sheath has been seen to diminish above  $\sim 15 \text{ GWd}\cdot\text{t(U)}^{-1}$  [54]. Further, bundles tested at  $\sim 20 \text{ GWd}\cdot\text{t(U)}^{-1}$  using CANLUB have not shown promising performance; all of the outer elements tested at  $\sim 20 \text{ GWd}\cdot\text{t(U)}^{-1}$  failed due to what are believed to be SCC failures [55]. These initial research efforts point towards the need to improve I-SCC mitigation strategies before power outputs can be increased from current CANDU fuel.

#### 1.8.5 Increasing the flexibility of CANDU units

Currently, the CANDU units operating in Ontario largely serve as base load producers. A method for increasing the flexibility of the NPPs would be to make the core itself more manoeuvrable, allowing for frequent changes in reactor power (*e.g.*, load following).

As mentioned before, the failure rates for fuel bundles are 0.01% in Canada since the implementation of the CANLUB sheath coating alongside adjusted fuel management procedures and improved quality assurance. Thus, the performance of the fuel within the average discharge burnup levels of  $7\text{-}9 \text{ GWd}\cdot\text{t(U)}^{-1}$  has been excellent since the change to CANLUB and less aggressive power ramps.

Tayal *et al.*, analyzed the results of the cycling load following test in the CANDU Embalse reactor in Argentina\* and the CANDU Bruce-B reactors in Canada† [31]. During these tests, both reactors still exhibit a fuel defect rate of 0.1%. Further, fuel that underwent load-following experiments did not exhibit any significant difference in the amount of fission gas being released when compared to fuel that did not undergo load-following while at similar burnups and power levels. While there has not been an increase in failure rates observed experimentally, moving to a load-

---

\* Cycled between 70 and 100% of full power,  $\sim 35$  times a week for lifetime of fuel.

† Cycled between 10 and 50% of full power,  $\sim 35$  times.

following schedule would surely introduce long-term loading effects that would have to be fully understood before being implemented in a commercial reactor.

## **1.9 Investigating Alternative Stress Corrosion Cracking Mitigation Strategies**

The current set of I-SCC mitigation strategies need to be improved to allow currently operating CANDU units to move to higher burnups or a more flexible fuelling schedule (*e.g.*, a form of load following). Elevated burnups would allow the units to extract more revenue without making significant changes to the units, while flexible fuelling schedules would allow the units to be more responsive to the electrical demand of the province. More flexible fuelling schedules would in turn lead to increased revenue, as units would be able to conserve some or all their production when demand is lower and, thus, extract higher revenues.

One alternative I-SCC mitigation strategy that could help facilitate these changes would be improving the protective coating on the interior surface of the sheath, as CANLUB has been proven to be ineffective at higher burnups [39].

### **1.9.1 RMC I-SCC Mitigation Research Program**

A series of experimental programs have been completed at RMC to investigate the mechanism of I-SCC and potential mitigation strategies for CANDU reactors. Lewis *et al.*, discussed mitigation strategies that attempt to improve the effectiveness of inner sheath coatings based on the two factors that are believed to be currently preventing I-SCC in CANDU reactors [2].

1. The ability of CANLUB to chemically capture corrosive elements from the environment and
2. The protective ability of the oxide layer that forms on the sheath.

The work of Lewis *et al.*, was then expanded upon with experimentally based investigations performed by Quastel *et al.*, and Farahani *et al.*, with research that was presented at the 12<sup>th</sup> International Conference on CANDU Fuel [56,57]. Quastel *et al.*, tested statically loaded slotted rings in sealed ampoules with iodine and controlled amounts of oxygen to investigate the theorized restorative properties of oxygen [56]. These static loading experiments form the base for the experimental procedure described in Section 3, including the design of the deflection measurement apparatus discussed in Section 3.5. The research from Farahani *et al.*, also performed static loading experiments, but on rings with various commercial protective coatings applied to the sheathing surface. This research explored the composition of the

different coatings as well as their mechanical properties after being statically loaded at high temperatures in the absence of iodine. The results from this investigation found Pyromark™ as the coating most worthy of further investigation (including iodine testing) [57].

It is at this point in the research program that the author of this thesis began contributing to the research efforts at RMC. The experiments completed by the author, which are presented in Section 4, attempt to set the baseline for all following I-SCC static loading investigation by performing an extensive set of baseline experiments investigating temperature, iodine, and stress and how they relate to I-SCC. From these experiments a well-defined baseline was developed for future mitigation experiments to be compared against. The author of this thesis completed a set of experiments investigating the mitigation properties of controlled amounts of alkali and alkaline earth metal oxides, as hypothesized by Lewis *et al.*, as well as a set of experiments furthering the research of Quastel *et al.*, on oxygen additions. As part of the oxygen investigation, a unique system was developed by the author of this thesis to control the small amounts of oxygen required in the experiments (see Section 3.4.1).

The author of this thesis left RMC to pursue full-time employment after these experiments were completed. The results from the experiments completed up until the departure of the author of this thesis were presented as a conference paper [58]. Further, while this thesis was being completed research efforts at RMC continued and two research papers were published using some results from this thesis by Ferrier *et al.*, [38,59]<sup>‡</sup>, as well as the experimental procedure described in this thesis. The first paper examined Pyromark and CANLUB through static loading experiments developed for the research described in this thesis. Baseline results from this thesis were used for comparison when analyzing the slotted ring results. The results from these experiments, as well as the result from the experiment performed to investigate the elemental compositions of CANLUB and Pyromark, are presented in Section 4.5 as part of this thesis. The second paper also utilized the static loading procedure described in this thesis, but this paper progressed the experiments on dopant additions. This thesis investigated the ability of Na<sub>2</sub>O and CaO dopants to mitigate I-SCC.

---

<sup>‡</sup> Note the author of this thesis was a co-author and contributor to these publications.

The following section discusses the theory behind the slotted ring experiments, as well as the theory behind the potential mitigation mechanisms that are described in this thesis.

## 1.10 Slotted Ring Experiment

All of the static loading experiments completed at RMC, as listed in the previous sub-section, are a modified version of the I-SCC using static loading developed by Wood *et al.*, which uses Zircaloy wedges on slotted rings [1]. The rings used by Wood *et al.*, were cut from Zr-4 fuel sheaths and slotted longitudinally. These slots can be then stressed by opening the slot further. This creates a maximum tensile stress on the inner surface of the tube directly opposite from the slot. This stress is created to simulate the stress experienced by CANDU fuel sheathings during operation. The analytical maximum tensile stress,  $\sigma_A$ , experienced at the inner surface opposite of where the slotted ring is being stressed, is given by Equation 2 [60]:

$$\sigma_A = \frac{Et(w - w_0)(1 + \cos \alpha)}{2R^2\{(\pi - \alpha)(1 + 2 \cos^2 \alpha) + 1.5 \sin 2\alpha\}} \quad \text{Equation 2}$$

This is a formula for bending stress that is valid while the ring is being elastically loaded. In it,  $E$  is the Young's Modulus,  $R$  is the radius,  $w$  is final slot position,  $w_0$  is the initial slot opening,  $\alpha$  is half of the angle of the slot in degrees, and  $t$  is the thickness of the ring. As the half-angle value approaches zero this equation can be simplified to approximate maximum tensile stress that is shown in Equation 3 [61].

$$\sigma \approx \frac{Et(w - w_0)}{3\pi R^2} \quad \text{Equation 3}$$

### 1.10.1 Static Loading

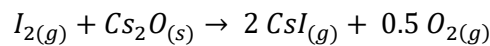
Wood developed a static loading procedure for testing slotted rings. The method involves placing the rings on Zircaloy wedges of a known width to create the static loading. The rings and wedges are placed in a vacuum pumped capsule and the environment is raised to a high temperature with a specific amount of iodine introduced. This experiment has proven to be useful because it is very easy to control

several factors that are worth investigating, namely: (i) the stress level can be managed through the size of the wedges, (ii) the temperature is easily controlled through the furnace, (iii) the amount of iodine can easily be varied, and (iv) the amount of time spent in the furnace can be controlled. Another advantage of this experiment is that since the iodine does not interact with glass, it is possible to determine the amount of iodine required to reach a desired concentration based on the surface area of the rings and wedges being used.

One of the issues with the static loading test is that the stress is applied before the samples were introduced to a corrosive environment at temperature. The applied stress continuously relaxes during this time, which makes it difficult to analyze the effects of applying initial stresses in a corrosive environment. Another disadvantage with this method is that I-SCC is a dynamic process and a different method is required to analyze the effects of dynamic loading on samples.

### 1.10.2 Alkaline Oxide Additives in CANLUB

Lewis *et al.*, postulated that the impurities within CANLUB might be chemically sequestering the iodine, so that iodine cannot interact with the sheath [2]. For example, including higher concentrations of elements that can bond with iodine, such as cesium oxide (Cs<sub>2</sub>O), calcium oxide (CaO), or sodium oxide (Na<sub>2</sub>O), could lead to a reduced amount of corrosive elements present in the fuel-to-sheath gap and introduce a small oxygen partial pressure that could repair any cracks in the protective ZrO<sub>2</sub> layer on the sheath (Equation 4).



Equation 4

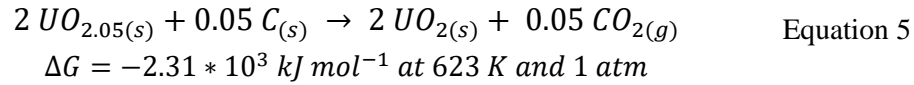
$$\Delta G = -533 \text{ kJ mol}^{-1} \text{ at } 600 \text{ K and } 1 \text{ atm}$$

The negative value for Gibb's free energy change indicates that Cs<sub>2</sub>O will preferentially interact with the available iodine to form CsI. However, it has been shown that CsI will dissociate when irradiated, which may lead to the iodine vapour being re-released back into the fuel-to-sheath gap. Thus, experiments will need to be performed with radiation present to confirm the feasibility of these additives.

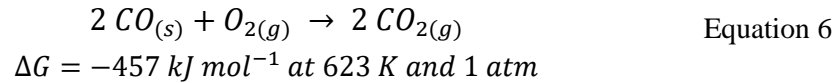
### 1.10.3 Inclusion of Oxygen

Quastel *et al.*, completed a limited number of experiments at RMC that were also based off the static loading procedure created by Wood *et al.*, to investigate the possible reparative properties of oxygen [1, 56]. The tests introduced known amounts of oxygen gas into ampoules as well as hyper-stoichiometric UO<sub>2+x</sub> (where *x* is the deviation from stoichiometric UO<sub>2</sub>) with dried graphite. UO<sub>2+x</sub> fuel could be

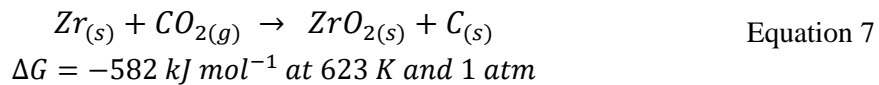
reduced by carbon from coatings to create both carbon monoxide and carbon dioxide (Equation 5).



The negative change in Gibbs free energy for this reaction indicates that this reaction is thermodynamically favourable in the forward direction and thus could lead to increased amounts of carbon dioxide in the fuel-to-sheath gas. The carbon monoxide that is also being produced by the interaction between carbon and the fuel could also create carbon dioxide when reacting with oxygen in Equation 6.



As these two reactions release carbon dioxide into the fuel-to-sheath gap, the carbon dioxide is free to move to any Zircaloy exposed from cracks in the oxide layer and help repair the oxide layer as shown in Equation 7.



The preliminary results from Quastel *et al.*, suggest that oxygen, either through oxygen gas or  $\text{UO}_{2+x}$ , may be providing some protection from iodine corrosion. It is also believed that graphite may be an important part of the mechanism of repairing the oxide layer.

## 2 Goals of Research

This thesis first describes the investigation and quantification of the effects of the three main baseline factors involved in inducing I-SCC, namely – *induced stress, temperature, and the corrosive environment*.

Next, the thesis describes the testing in two phases of the hypothesized I-SCC mitigation strategies:

- The first mitigation method to be described involves introducing elevated levels of oxygen into the experiment, ensuring the presence of excess oxygen. This allows for the relationship between the oxide layer repair and I-SCC mitigation to be investigated.
- The second hypothesized mitigation method described is the introduction of alkali earth metal oxides, specifically  $\text{Na}_2\text{O}$  and  $\text{CaO}$ , into the experiments. The desired interaction is for the corrosive  $\text{I}_2$  to become chemically sequestered in a stable compound with sodium or calcium. Further, it is postulated that the released oxygen molecules by the dissociation of the oxides (*i.e.*,  $\text{Na}_2\text{O}$  and  $\text{CaO}$ ,) may be capable of aiding the oxide layer and its suggested protective properties.

Further, select results from two Ferrier *et al.*, papers [38,57], which the author of this thesis contributed to, are also presented. These experiments test the I-SCC mitigation capabilities of CANLUB and an additional coating, Pyromark.

Thus, these data attempt to define the corrosive effects of I-SCC on Zr-4, and then attempt to mitigate these effects. The goal is then to gain insights into which I-SCC mitigation strategies warrant further investigation.

The following section explains the experimental design that was developed to meet the goals listed above, including an explanation of how the experiments were performed. The results from the experiments are then presented and analyzed, with the baseline I-SCC results presented first, followed by the theorized mitigation strategies. A discussion section is then presented expanding upon the results and analysis. Finally, conclusions are drawn, and future recommendations are provided.

### **3 Experimental Apparatuses and Procedures**

This section describes the experimental design of the research and the theory behind the organization of the experiments, followed by a thorough explanation of the experimental procedure used to perform the static loading experiments and deflection measurements.

#### **3.1 Terminology**

The experiments of this research have two different types of results: deflection measurements and final slot sizes. More details on these results, what they are attempting to quantify, and how they are measured are provided in the following subsections.

The affect of different variables on these results is what is being investigated. The first three variables establish the corrosive environment, while the following variables attempt to mitigate this corrosive environment. The results are analyzed through multivariable linear regression analyses. Moving forward all inputs into regression analyses will be referred to as variables while deflection results and slot size results will be examined separately.

#### **3.2 Experimental Matrix Design**

The experimental matrix is to establish baseline levels of I-SCC degradation, potential mitigation strategies are then studied in order to identify strategies that warrant further investigation (*i.e.*, oxygen partial pressures and dopants).

The matrix shown in Table 8 shows the experiments completed; varying levels of  $I_2$ ,  $Na_2O$ , and  $CaO$  are included in ampoules at two different temperatures and controlled levels of  $O_2$  gas are introduced to some ampoules. The matrix is designed in such a way that linear regressions can be completed on all variables, wherein quantitative evaluations of the effect of all variables can be determined alongside statistical confidence levels associated with each effect. Linear regression is performed on the results of post-experiment deflection measurements. The theory behind slotted ring deflection measurements was outlined in Section 1.10.

The goal of this research is to establish a quantifiable level of I-SCC corrosion in slotted ring samples, then to test and evaluate mitigation strategies against those baseline corrosion results. Experiments listed in Table 8 are completed with this framework in mind, and it is the same order that the results are presented and analyzed in Section 4. Section 4 also presents the analysis of the effect of wedge size on static loading results.

**Table 8: Static loading experimental matrix. Where N is the number of replicates. Wedge sizes were varied at each condition. See Appendix for full matrix and results.**

<b>N</b>	<b>Temperature / °C</b>	<b>Iodine / mg</b>	<b>O<sub>2</sub> Gas / Torr</b>	<b>Na<sub>2</sub>O / g</b>	<b>CaO / g</b>
9	23	0	0	0	0
24	300	0	0	0	0
16	375	0	0	0	0
23	300	255	0	0	0
8	375	255	0	0	0
23	300	1530	0	0	0
8	375	1530	0	0	0
16	300	1530	6	0	0
15	375	1530	6	0	0
8	300	1530	12	0	0
7	375	1530	12	0	0
15	300	1530	54	0	0
18	375	1530	54	0	0
8	300	1530	0	0.68	0
8	300	1530	0	0.68	0
8	300	1530	0	0.84	0
24	300	1530	0	0	0.08
24	300	1530	0	0	0.17
24	300	1530	0	0	0.25
8	300	1530	0	0	0.33
16	300	1530	0	0	0.34

The experiments listed in this matrix are used to analyze the effects of temperature, iodine, O<sub>2</sub> gas, Na<sub>2</sub>O, CaO, and wedge in terms of their relationship with I-SCC. A full list of the experiments performed and the results from the experiments found in the Appendix A,. The following subsections describe the process used for the experiments.

### **3.3 Slotted Ring Preparation**

Slotted rings (Figure 8) are cut from Zr-4 sheath tubes ( $13.10 \pm 0.05$  mm diameter) using a Buehler Isomet 1000 precision saw equipped with a diamond blade (151 mm diameter, 0.6 mm thickness). Specifically, each ring is cut to a  $5.00 \pm 0.05$  mm width, and subsequently slotted with a  $2.30 \pm 0.08$  mm opening. Rough and frayed

edges made by the cutting process are smoothed and polished using 320 and 600 grit silicon carbide paper. Finally, the slotted rings are ultrasonically cleaned in ethanol for 25 min to remove shavings and dust created during the cutting process.

### 3.4 Static Loading

A test procedure for static loading was developed based on the work of Wood *et al.*, [1] and Quastel *et al.*, [56]. The procedure involves fastening the slotted rings onto a Zr-4 wedge (Figure 8). Once the rings are fastened (Figure 9), the ring-wedge assembly is placed in a long cylindrical glass capsule, along with a small glass vial containing a known amount of iodine (Figure 10). A total of 4 rings could fit on each wedge, with two wedges being used per sample run.



Figure 8: Zr-4 slotted ring samples and a Zr-4 static wedge.



**Figure 9: Loaded slotted ring samples.**



**Figure 10: Glass vial containing iodine.**

The iodine vial features a gooseneck and contains a trace amount of argon. The fragile gooseneck makes it possible to break open the iodine vial with gentle agitation at the desired point in the experiment. The amount of iodine included in the vial is determined by selecting an iodine concentration to be investigated. The amount of iodine required could then be calculated by accounting for the total amount of Zr-4 surface area that is exposed to the iodine, both from the rings and the wedges.

The capsule containing the iodine vial and the loaded slotted rings are necked down using glass blowing techniques to create a narrow section (Figure 11). The necked capsule is then attached to a vacuum system to remove moisture and air from the capsule (Figure 12). The vacuum system consists of an Alcatel rotary pump, which is used initially to remove the bulk amount of oxygen from the ampoule. After a sufficiently low oxygen concentration remains in the capsule (pressure =  $10^{-2}$  Torr), a turbomolecular pump (Varian Turbo – V70D Macro Torr, Agilent Technologies) can safely pump down to a vacuum pressure of 7-30  $\mu$ Torr over an 18-24 h timeframe. After this pressure is achieved, an ampoule (containing the rings and

iodine vial) is flamed off the capsule from the necked region using a torch, thereby sealing the low vacuum pressure within the ampoule.



**Figure 11: Necked down glass ampoule.**



**Figure 12: Vacuum system for evacuating ampoules.**

At this point the iodine vials were ready to be broken away from the vacuuming assembly before being placed in the furnace as is seen in Figure 13. Once the furnace reaches its desired temperature, the combination of pressure and temperature causes the iodine to sublime into a purple gas, which is shown in Figure 14.



**Figure 13: Sealed ampoule with iodine capsule inside furnace before heating.**



**Figure 14: The purple glow of iodine vapour.**

The following subsection details the process developed by the author of this thesis to introduce  $O_2$  gas into the ampoules.

### **3.4.1 $O_2$ Additions**

The  $O_2$  addition experiments performed and presented use a valve system designed to allow small, controllable amounts of  $O_2$  gas into the experimental ampoules. These experiments are intended to determine whether  $O_2$  gas mitigates SCC, possibly by repairing cracks in the protective oxide layer. In addition, these experiments attempt to confirm previous results reported by Quasetl *et al.*, [56].

In  $O_2$  addition experiments, ampoules are vacuumed to 7-30  $\mu$ Torr and then re-filled with  $O_2$  gas to specified pressure levels before flame-sealing the ampoule. The levels of oxygen utilized are 1, 2, and 9  $\mu\text{mol}_{O_2} \cdot \text{cm}^{-3}_{Zr-4}$ , which correspond to oxygen partial pressures of 6, 12, and 54 Torr, respectively.

The process of delivering  $O_2$  gas to an ampoule begins by connecting the ampoule to a pressurized gas tank (Air Liquide, Montreal) containing 99.999% pure  $O_2$  gas using a valve system (Figure 15) consisting of a three-way valve followed by two consecutive bleed valves. Placing two bleed valves in series allows for precise control of  $O_2$  gas flow into the ampoule.

During the initial process of vacuuming the ampoule, both bleed valves are fully opened and the three-way valve is directed to open atmosphere, allowing the system to be placed under vacuum all the way up to the three-way valve. Once the system reaches 7-30  $\mu$ Torr,  $O_2$  gas is used to flush the piping between the tank and the three-way valve, which is still open to the atmosphere (Figure 15A). At this point, the vacuum pump is turned off, the bleed valves are both closed, and the three-way valve is dialled to direct the flow of oxygen toward the ampoule and closed bleed valves.

The bleed valves are opened slightly to allow a controlled flow of O<sub>2</sub> gas into the valve system and ampoule (Figure 15B). A pressure gauge, downstream of the bleed valves, is monitored until the pressure reaches the desired level. After which, the O<sub>2</sub> gas supply is turned off and the ampoule is promptly flame-sealed, detached, and placed in a tube furnace for five days at 300 °C.

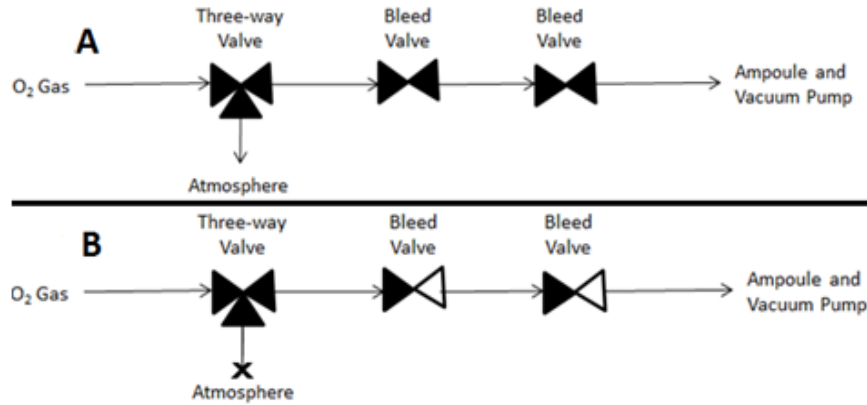


**Figure 15A: First valve configuration.** O<sub>2</sub> gas is flushing air out of system up to three-way valve. The vacuum pump is removing air up to the three-way valve, including both bleed valves. **B: Second valve configuration.** O<sub>2</sub> gas is now free to flow through the consecutive bleed valves.

The following subsection details how the second I-SCC mitigation method tested, alkali earth metal oxide additives, were introduced into the experiments.

### 3.4.2 Dopant Additions

The method to introduce controlled amounts of alkali earth metal oxides, Na<sub>2</sub>O and CaO, into the ampoules is the same as that for I<sub>2</sub>. That is, the desired amount is placed into a small glass vial with a gooseneck. Once the ampoule is at a sufficiently low pressure, the goosenecks are broken by agitating the ampoule.

## 3.5 Deflection Measurements

A previously designed slotted ring deflection testing apparatus was used to measure the severity of corrosive attack on rings after static loading as outlined by Quastel *et al.*, [56]. According to Quastel *et al.*, Equation 8 is derived from the unit load method and describes the expected deflection,  $D_y$  (m), of a ring sample when under a weight force of  $F_y$  (N) where  $l$  is the width of the ring (m),  $E$  is the young's modulus, and  $R$  is the radius (m).

$$D_y = \frac{36\pi R^3 F_y}{E l t^3} \quad \text{Equation 8}$$

Since the deflection is inversely proportional to the cube of the ring thickness ( $t$ ), any process that narrows the ring will greatly increase the expected ring deflection under an applied load. An example of such a process is the surface degradation experienced in a corrosive environment, whereby one may correlate deflection increases to enhanced surface degradation. Figure 16 displays scanning electron microscopy (SEM) images of a Zr-4 surface before and after corrosion testing. The SEM images were captured using an FEI Nova NanoSEM 450. The effect of the corrosive material on the surface of the ring can be seen in the form of white blotches.

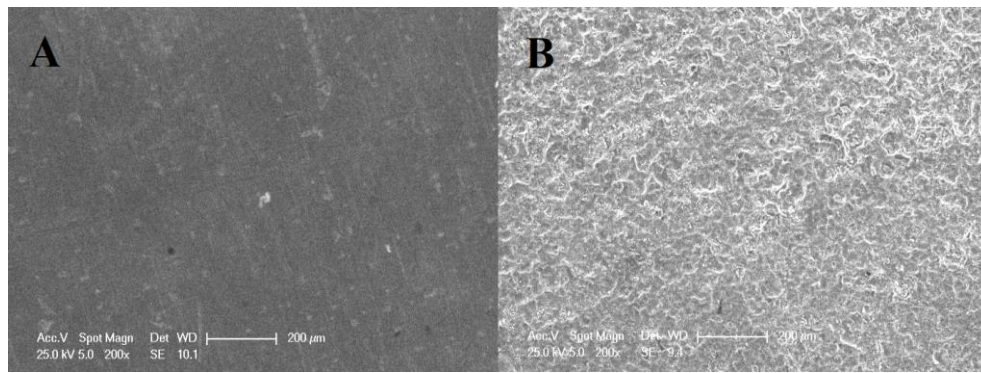


**Figure 16: SEM images of (A) a Zr-4 ring surface after being exposed to 300 °C on a 9 mm wide wedge and (B) A Zr-4 ring surface after being exposed to the same condition as (A), except 1530 mg of I<sub>2</sub> were introduced to the experiment.**

To quantify the amount of surface degradation (*e.g.*, thickness reduction) experienced by corrosive attack, ring deflections are measured using the deflection apparatus built at the RMC. The apparatus (Figure 17) operates by attaching a ring sample to both the static and lever jaw. At the end of the lever, a load force is attached and the corresponding deflection corresponds to the amount of degradation the ring has experienced. All measurements are zeroed using a 5 g weight and are repeated with 20, 50, and 100 g weights. An OMEGA LD400-1 linear displacement transducer was used to record the vertical displacement of the specimen. The transducer receives power from a HP 6236B power supply. The transducer voltage signal is converted to a deflection distance using a LabVIEW program and recorded using a National Instruments NI 9205 data acquisition card in a NI cDAQ-9172 chassis. An overview of the apparatus is shown in Figure 17.

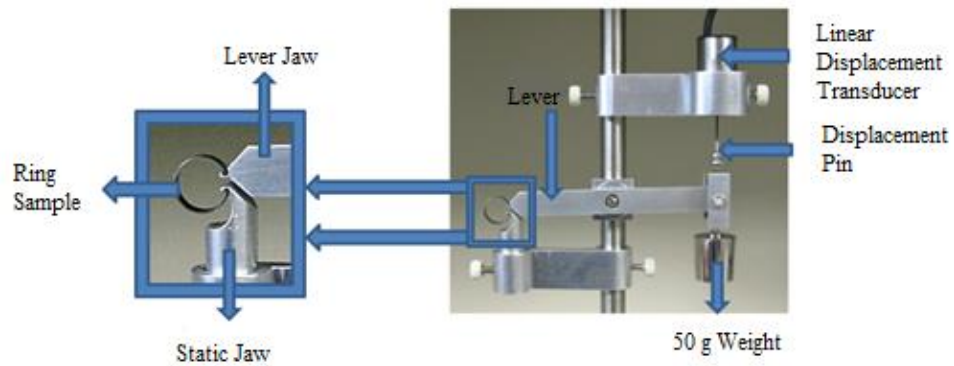


**Figure 17: Apparatus for performing deflection measurements, adapted from [56].**

After deflection measurements are recorded, the final slot openings of the samples are also recorded and compared to their initial opening.

The following section presents the analysis of the results from the completed I-SCC slotted ring experiments.

## **4 Results and Analysis**

The goal of the research is to evaluate the potential I-SCC mitigation strategies for further investigation. To accomplish this, the experiments first establish a baseline level of corrosion. Next, various I-SCC mitigation strategies are introduced to evaluate any ability to mitigate the corrosion in question. All rings in question are prepared using the procedure outlined in Section 3.3 and are confirmed to be within the tolerances detailed in the same section.

Deflection measurements are used to quantify the level of degradation experienced by a Zr-4 slotted ring caused by I-SCC. Slot size measurements are used to investigate stress relaxation effects in Zr-4 and how various variables influence final slot size results. SEM images are also taken and are used to support the quantitative results.

### **4.1 Static Loading Results**

The first sets of data investigated are three batches of baseline rings to investigate the repeatability of the slotted rings being used for all the following experiments (Section 4.2 and onwards).

A dataset was then collected to investigate the three main variables of I-SCC and how they affect both deflection results and slot size results. The three variables investigated are: stress level (wedge size), temperature, and iodine amount. It can be determined from these results which of these three variables affect deflection and slot size results, and by how much. With the understanding gained from these baseline experiments, it is possible to assess the I-SCC mitigation strategies that are under investigation.

Experiments are performed to investigate how the inclusion of O<sub>2</sub> gas affects I-SCC in slotted rings of Zr-4 through the reparation of the protective oxide layer. The goal of these experiments was to isolate the effect of O<sub>2</sub> gas on I-SCC mitigation. This allows for the investigation into chemicals featuring oxygen to be analyzed with an understanding of the contribution to I-SCC mitigation caused by oxygen.

Experiments are undertaken to investigate the I-SCC mitigation capabilities of both an alkaline metal oxide and an alkali earth metal oxide (Section 4.4). The compounds investigated are Na<sub>2</sub>O and CaO. A regression analysis is performed on deflection results that contained controlled amounts of the oxides in question to gain a quantifiable understanding of how these oxides influence I-SCC mitigation.

## 4.2 Analysis of Baseline Slotted Rings

The analysis features three batches of baseline rings that are cut from different Zr-4 tubes. Each batch contains three rings with dimensions within the tolerances discussed in Section 3.3. The slotted rings are not stressed, exposed to high temperatures, nor exposed to any type of corrosive environment. The slotted rings are subjected to mass loads of 45 and 95 g (using the apparatus discussed in Section 3.5) and the corresponding deflections are recorded. The width of each slot is then measured using a caliper. This analysis is performed to understand the repeatability and consistency of measurements. Table 9 displays the average deflections and slot size for each batch, with an average result across all nine rings shown in italics.

**Table 9: Average deflections and slot sizes for three distinct batches of slotted ring samples solely subjected to the cutting process. Each batch contained 3 samples. Numbers in bold express the average deflections and slot size for all nine rings tested. The error attached to each value is one standard deviation.**

<b>Batch</b>	<b>45g Deflection / mm</b>	<b>95g Deflection / mm</b>	<b>Slot Size / mm</b>
1	<b><i>0.42 ± 0.04</i></b>	<b><i>0.80 ± 0.03</i></b>	<b><i>2.29 ± 0.04</i></b>
2	<b><i>0.37 ± 0.03</i></b>	<b><i>0.78 ± 0.02</i></b>	<b><i>2.35 ± 0.02</i></b>
3	<b><i>0.41 ± 0.03</i></b>	<b><i>0.82 ± 0.02</i></b>	<b><i>2.30 ± 0.02</i></b>
<i>Average</i>	<b><i>0.40 ± 0.04</i></b>	<b><i>0.80 ± 0.02</i></b>	<b><i>2.31 ± 0.04</i></b>

The average deflection results for each batch are all within one standard deviation of one another for both the 45 and 95 g deflection. The slot size results are also within one standard deviation of one another. It is important that there is repeatability in results taken from three separate sources of Zr-4, as this allows for further experiments to be performed without fear of introducing a systematic error through the slotted rings. To quantify whether any of the three batches were distinct from one another for any of the metrics used (45 g deflection, 95 g deflection, and slot size) analyses of variances (ANOVA) are performed. ANOVA [62] is a series of statistical calculations used to determine if more than two datasets are distinct from one another. The ANOVAs completed on the three batches above are performed using the data analysis toolpak in Microsoft™ Excel [63]. The resultant p-values from the ANOVAs can be seen in Table 10. Table 10 displays solely p-values as that is the most important output of this analysis for establishing statistical significance. Full ANOVAs for the baseline rings are shown in Appendix Section 9.1.

**Table 10: Associated  $p$ -values from ANOVA analyses of baseline batches of slotted rings.**

<b>Metric</b>	<b><math>p</math>-value</b>
45 g Deflection	0.22
95 g Deflection	0.19
Slot Size	0.11

The  $p$ -values are used to express the probability of whether the batches in question are distinct from one another. The accepted threshold required to state that there is a distinct dataset being analyzed with a 95% confidence level is if the  $p$ -value is less than 0.05. None of the  $p$ -values in Table 10 meet this threshold (all  $> 0.05$ ), thus it can be stated that all three batches of baseline ring samples analyzed are consistent in terms of 45 g deflection, 95 g deflection, and slot size.

This finding indicates it can be considered that there are no inconsistencies introduced into the results from using multiple sources of Zr-4. The results in Table 9 also display baseline variance level that can be expected from the slotted rings; the starting variance seen in 45 g deflection, 95 g deflection, and slot size results is on the order of  $\sim 0.05$  mm according to the standard deviations seen in Table 9.

#### **4.2.1 I-SCC Static Loading Results**

Experiments are performed to gain an understanding of how the three main variables of I-SCC affect slotted rings of Zr-4. The three variables in question are: amount of  $I_2$  included, temperature, and strain level (controlled through the width of static wedges). Table 11 displays the experimental conditions for this subset investigation.

**Table 11: Summary of I-SCC static loading conditions (N = number of samples). Note that there are more samples on taken with 9 mm wedges. Experiments were limited by available wedges and there were multiple 9 mm wedges, including one with a bevel that better secured the rings for these wedges. It is shown from experiments that wedge sizes do no affect deflection results, so wedge size was varied freely which led to large sample sizes with 9 mm wedges.**

<b>Iodine ± 10 / mg</b>	<b>Wedge ± 0.05 / mm</b>	<b>Temperature ± 10 / °C</b>	<b>N</b>
1530	6	300	4
1530	7	300	4
1530	9	300	12
1530	12	300	4
1530	9	375	4
1530	12	375	4
255	4.5	300	4
255	6	300	4
255	7	300	4
255	9	300	8
255	12	300	3
255	6	375	4
255	7	375	4
0	4.5	300	4
0	6	300	4
0	7	300	4
0	9	300	8
0	12	300	4
0	6	375	4
0	7	375	4
0	9	375	4
0	12	375	4

This dataset features a total of 103 ring samples collected across 22 distinct test conditions.

#### ***4.2.1.1 I-SCC Static Loading Deflection Measurements***

To develop a more complete and quantifiable understanding of how temperature, wedge size, and iodine level affect deflection results, a multivariable linear regression is performed using Microsoft Excel™. The regression is performed to model the deflections experienced by each ring when loaded with a 95 g mass. A

summary of the data used for the regression is displayed in Table 11. The statistics for each variable from the preliminary regression results are shown in Table 12.

**Table 12: Preliminary regression results from I-SCC deflection results.**

<b>Variable</b>	<b>Coefficients</b>	<b>Standard Error</b>	<b><i>p</i>-value</b>
<b>Iodine / mm mg<sup>-1</sup></b>	0.0001	1.4 x 10 <sup>-5</sup>	4.7 x 10 <sup>-16</sup>
<b>Temperature / mm °C<sup>-1</sup></b>	0.0006	0.0003	0.02
<b>Wedge Size / mm mm<sup>-1</sup></b>	0.002	0.004	0.7

The *p*-value in Table 12 represents the likelihood of a variable not having a significant linear effect on deflection results. This value must be less than 0.05 for the variable to be accepted into the model at the 95% confidence level. Since the *p*-value for wedge size was too high (0.7 > 0.05) it was removed from the model. The regression was updated with temperature and iodine as the variables of interest in Table 13.

**Table 13: Updated regression results from I-SCC deflection results.**

<b>Variable</b>	<b>Coefficients</b>	<b>Standard Error</b>	<b><i>p</i>-value</b>
<b>Iodine / mm mg<sup>-1</sup></b>	0.0001	1.3 x 10 <sup>-5</sup>	3.9 x 10 <sup>-17</sup>
<b>Temperature / mm °C<sup>-1</sup></b>	0.0006	0.0003	0.02

All of the variables in the updated regression results have a *p*-value of < 0.05, which indicates that they can all be accepted with 95% confidence. Figure 18 through Figure 20 display the deflection results against each specific variable, with error bars representing a standard deviation from the results in either direction. These figures are used to visualize/confirm the results from the regression analysis. There appears to be an increase in deflection at high levels of iodine (Figure 18), a possible increase in deflection at higher temperatures (Figure 19), and no apparent effect on deflection from changes in wedge size (Figure 20). These observations correspond well with the *p*-values found in the original regression results. In light of the large overlap in error bars in Figure 19, a two-tailed, type three, *t*-test was performed [64] for the temperature results to confirm that the ring deflections at 300 °C and 375 °C are distinct (at a 95% confidence level).

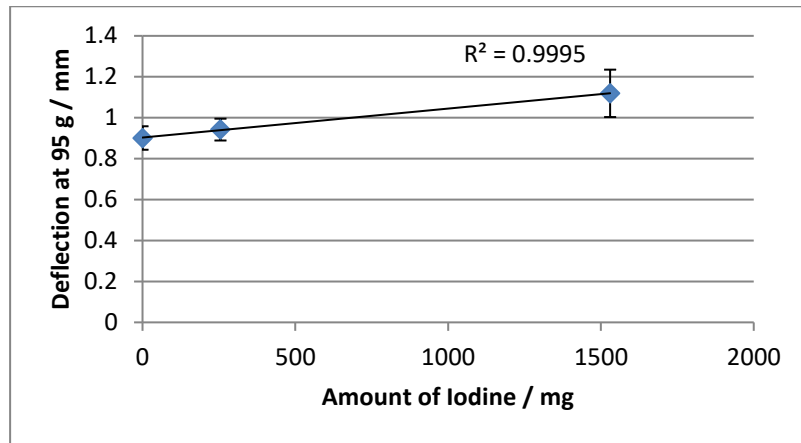


Figure 18: Average deflection results at 300 °C of ring samples on 9 mm wedges vs. iodine (error bars = 1 standard deviation).

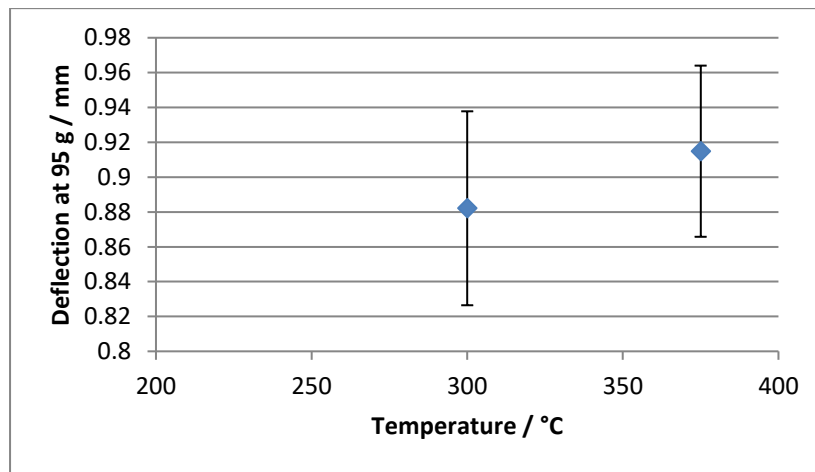
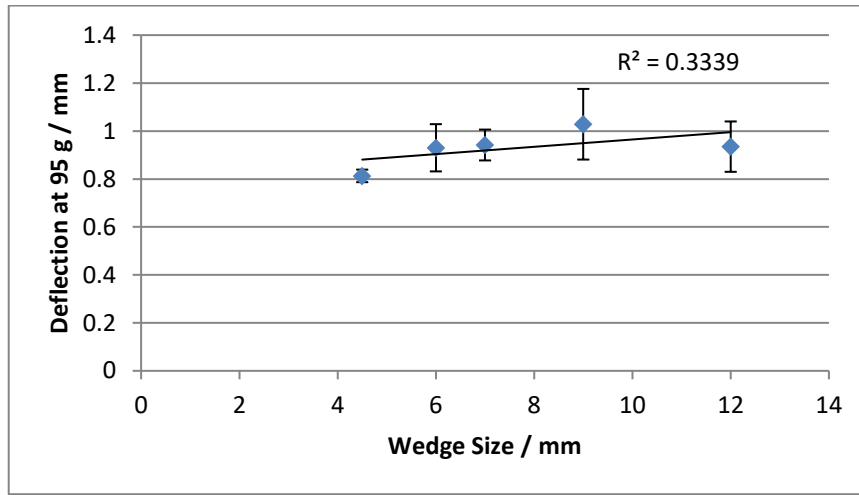


Figure 19: Average deflection results for all samples tested without iodine vs. temperature (error bars = 1 standard deviation). Line of best fit and  $R^2$  are not shown as they would be invalid across only two data points.



**Figure 20: Average deflection results for experiments performed vs. wedge size (error bars = 1 standard deviation).**

The regression analysis shown in Table 13 displays the likelihood that temperature and the amount of  $I_2$  present both significantly affect 95 g deflection results. When examining Table 13 it is less clear what actual expected changes in deflections could be expected from the two variables, as their coefficients appear as very small numbers in different units. The coefficients produced predict an increase in deflection of  $0.13 \pm 0.02$  mm when the amount of  $I_2$  present is increased from 255 mg to 1530 mg. If the temperature was increased in an experiment from 300 °C to 375 °C the regression analysis predicts an increase in deflection of  $0.04 \pm 0.14$  mm. The large error value associated with the predicted change in deflection results from increasing the temperature provides a better understanding of the reliability of the effect of temperature on deflection results. While the effect of temperature is strong enough that it can be seen through a regression analysis featuring a large number of samples it is much more difficult to isolate the effect of temperature on a case-to-case basis. The conclusions that can be drawn from this dataset with respect to deflection results are as follows:

- Wedge size does not affect deflection results in standard I-SCC slotted ring experiments;
- Increasing the temperature of an experiment likely has a small, unreliable effect on deflection results in standard I-SCC slotted ring experiments; and
- The amount of  $I_2$  present in an ampoule has a large, reliable effect on the deflection results in standard I-SCC slotted ring experiments.

These understandings form a baseline that static loading tests examining I-SCC mitigation strategies are compared against. A similar understanding is desired in terms of how the three main variables affect the final slot size of slotted rings is explored in Section 4.2.1.2.

#### 4.2.1.2 I-SCC Static Loading Slot Size Measurements

Using the dataset summarized in Table 11 the effects of the three main variables of I-SCC on the slot sizes of Zr-4 slotted rings were investigated. A regression analysis is performed on the slot size results and the results for the variables are shown in Table 14.

**Table 14: Regression results from I-SCC slot size results**

<b>Variable</b>	<b>Coefficients</b>	<b>Standard Error</b>	<b>p-value</b>
<b>Iodine / mm mg<sup>-1</sup></b>	0.0002	0.0001	0.022
<b>Wedge Size / mm mm<sup>-1</sup></b>	0.9335	0.0220	2.9 x 10 <sup>-47</sup>
<b>Temperature / mm °C<sup>-1</sup></b>	0.0232	0.0014	1.3 x 10 <sup>-19</sup>

The p-values that correspond to temperature and wedge size are both very low (p-value  $\ll$  0.5). This means it can be stated that both variables have a statistically significant effect on final slot size results in Zr-4 slotted ring samples. The p-value for I<sub>2</sub> is also lower than the threshold required to be deemed a statistically significant variable at the 95% confidence level (p-value < 0.5). The proximity of iodine to the 0.05 threshold justifies further investigation into the effects of I<sub>2</sub> on final slot size.

With regards to the relative effect of each variable on slot size results, wedge size appears to be the driving force in terms of the final slot size of a slotted ring. Using the coefficients listed in Table 14 one can calculate the predicted change in final slot size from varying the different variables. This can shed light on the relative effects of all the variables, for example the predicted difference between using a 4.5 and 12.5 mm wedge is an increase in slot size  $7.0 \pm 0.3$  mm. The effect on slot size moving from 255 to 1530 mg of I<sub>2</sub> is predicted to be  $0.3 \pm 0.2$  mm, while the predicted effect of running an experiment at a temperature of 375 °C instead of 300 °C is  $1.7 \pm 0.7$ . From these results the following conclusions can be drawn with regards to the effects of I-SCC variables on the final slot size of Zr-4 slotted rings:

- Increasing amounts of  $I_2$  likely leads to small increases in the final slot sizes of Zr-4 slotted rings in I-SCC tests;
- Wedge size has a very large, reliable effect on the final slot sizes of Zr-4 slotted rings in I-SCC tests, where larger wedge size lead to larger final slots; and
- The temperature of the static loading test has a moderate, reliable effect on the final slot sizes of Zr-4 slotted rings in I-SCC tests, where increasing the temperature increases the predicted size of the slot.

With an understanding of how the three main variables of I-SCC (temperature, wedge size (strain level), and amount of  $I_2$ ) affect slot size and deflection results I-SCC mitigation strategies can be examined and compared back to the results found in Section 4.2. One of the main takeaways from these results that will be carried forward is the fact that wedge size (*i.e.*, strain level) does not appear to be a significant factor in influencing final deflection results. While the width of the wedges unsurprisingly is a driving factor in the final slot size of the rings (alongside the temperature of the experiments), slot size is a secondary analysis technique compared to deflection measurements. This is because deflection measurements are more representative of the main goal to understand corrosion mitigation properties. As such, the following experiments are more focused on the deflection results and thus there is less focus on varying the sizes of the wedges at each upcoming condition. Final slot sizes will still be recorded and analyzed, and varying wedge sizes will still be used to ensure these factors do not have an unexpected influence on the results. Moving forward, the vast majority of experiments are performed at 300 °C with 1530 mg of  $I_2$  present (some experiments were performed at 375 °C in the  $O_2$  gas experiments to look for any potential interaction effect between  $O_2$  gas and temperature). As wedge size has been shown to have no effect on final deflection results wedge sizes are varied freely. Using these understandings, the first I-SCC mitigation strategy investigated involved introducing  $O_2$  gas into ampoules.

### 4.3 Oxygen Additive Static Loading Results

An investigation was performed to examine the effect of  $O_2$  gas on I-SCC of slotted rings of Zr-4. These experiments were designed to gain an understanding of how pure  $O_2$  affects I-SCC mitigation. A dataset is collected with ring samples that are placed on a static wedge and placed into a hot, corrosive environment with varying amounts of  $O_2$  gas introduced. Table 15 summarizes these conditions and displays the baseline dataset used to compare against  $O_2$  gas results.

**Table 15: Test conditions for investigation into effects of O<sub>2</sub> gas on I-SCC. All experiments listed below were performed with 1530 mg of I<sub>2</sub> present.**

<b>Temperature / °C</b>	<b>O<sub>2</sub> Gas / Torr</b>	<b>N</b>
300 ± 10	0	24
375 ± 10	0	8
300 ± 10	6.0 ± 0.5	16
375 ± 10	6.0 ± 0.5	16
300 ± 10	12 ± 1	8
375 ± 10	12 ± 1	10
300 ± 10	54 ± 2	16
375 ± 10	54 ± 2	18

This dataset features a total of 116 ring samples collected across eight distinct test conditions. The following subsections, Sections 4.3.1 and 4.3.1.2, describe how O<sub>2</sub> gas affects deflection and final slot size results.

#### **4.3.1 Oxygen Additive Static Loading Deflection Measurements**

Figure 21 shows the deflection ( $D_y$ ) results for a 95 g mass-load for 116 distinct ring samples. Slotted ring samples are stressed on 6-12 mm wide Zr-4 wedges, with 1530 mg of I<sub>2</sub>, and heated at 300 °C or 375 °C with varying amounts of O<sub>2</sub> gas introduced into the ampoules. Based on the distribution of all results (Figure 21), one cannot readily determine if increasing the oxygen pressure significantly limits the extent of iodine attack. Therefore, to develop a more complete and quantifiable understanding of whether O<sub>2</sub> gas, temperature, and wedge size affect deflection results, a multivariable linear regression is performed using Microsoft Excel™. Results from the first regression (Table 16) include an intercept of 1.0 mm, standard error of 0.12, and a  $p$ -value of  $4 \times 10^{-14}$ .

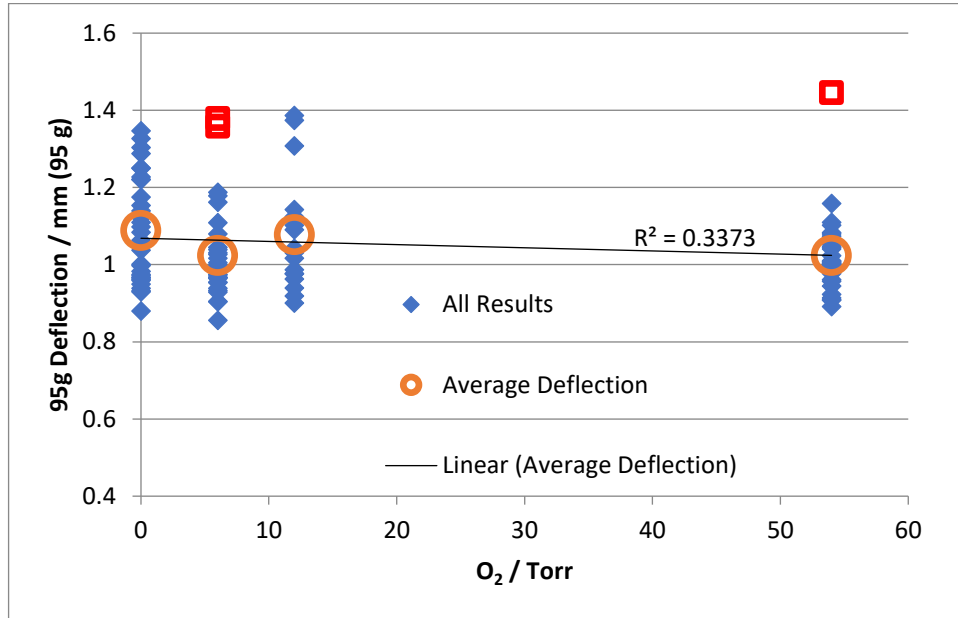


Figure 21: 95 g deflection results for all O<sub>2</sub> gas tests. Red squares denote outliers and orange circles display the average deflection at each O<sub>2</sub> level (excluding outliers). The trend line and R<sup>2</sup> value are based on average deflection values for each O<sub>2</sub> gas level.

Table 16: Preliminary oxygen gas regression results

Variable	Coefficients	Standard Error	<i>p</i> -value
Temperature / mm °C <sup>-1</sup>	3 x 10 <sup>-4</sup>	3 x 10 <sup>-4</sup>	0.32
O <sub>2</sub> Gas / mm Torr <sup>-1</sup>	-9 x 10 <sup>-4</sup>	5 x 10 <sup>-4</sup>	0.09
Wedge Size / mm mm <sup>-1</sup>	-6 x 10 <sup>-3</sup>	6 x 10 <sup>-3</sup>	0.30

From Table 16 it can be seen that both temperature and wedge size do not have a significant effect on deflections (*p*-value > 0.1) while the effect of oxygen gas is between the 95% and 90% confidence levels (0.05 < *p*-value < 0.1). Backwards elimination regression analysis requires the least significant factor that has a *p*-value greater than 0.05 to be removed from the analysis and to re-run the regression [65]. Temperature and wedge size are sequentially removed from the regression analysis as temperature had the highest *p*-value from the initial regression, and a secondary regression featuring only O<sub>2</sub> gas and wedge size as variables produce a *p*-value of 0.23 for wedge size. The final regression included an intercept of 1.07 mm, standard error of 0.02, and a *p*-value of 2 x 10<sup>-95</sup>. The final result for the O<sub>2</sub> gas variable is a coefficient of -8 x 10<sup>-4</sup> mm Torr<sup>-1</sup>, a standard error of 5 x 10<sup>-4</sup>, and a *p*-value of 0.13.

The  $p$ -value for O<sub>2</sub> gas is now outside of requirement for even a 90% confidence level ( $p$ -value > 0.1), which would not allow O<sub>2</sub> gas to be accepted as a statistically significant factor in terms of affecting deflection results. However, when inspecting the points in Figure 21, it can be seen that there are data points at each oxygen level that appear to be significantly higher than the rest of these data at said level of O<sub>2</sub> gas. In light of this, an investigation was performed to try and determine if any of these data points could be classified as outliers and removed from the dataset.

#### 4.3.1.1.1 Identification of statistical outliers

Tukey's method is used to search for data points that could be classified as outliers [66]. The process of Tukey's method begins by determining the first ( $Q1$ ) and third quartile ( $Q3$ ) values in a dataset.  $Q1$  represents the point where 25% of the dataset occurs below this value, whilst  $Q3$  is the point where 25% of the dataset occurs above this value. For this investigation, built-in Microsoft Excel™ functions are used to determine  $Q1$  and  $Q3$  for each level of O<sub>2</sub> gas addition. The interquartile range,  $IQR$ , is determined using  $Q1$  and  $Q3$  as shown in Equation 9.

$$IQR = Q3 - Q1 \quad \text{Equation 9}$$

The upper and lower fences values are determined using Equation 10 and Equation 11.

$$\text{Lower Fence} = Q1 - (IQR * 3) \quad \text{Equation 10}$$

$$\text{Upper Fence} = Q3 + (IQR * 3) \quad \text{Equation 11}$$

Results that fall outside the range set by the lower and upper fence can be categorized as outliers. It should be noted that the value used to multiply the  $IQR$  by is often 1.5 instead of 3. For this analysis, a higher value is selected to provide a more conservative approach in determining outliers. This approach is used because the experimental method used in this research yielded high variance results and a less conservative approach suggests that a large amount of data should be removed. The conservative approach led to the removal of three data points: two points from the 6 Torr results; and one point from the 54 Torr results (depicted by red squares in Figure 21). It is unclear what caused these outliers to occur as each result came from separate tests where a single ring displayed significantly higher deflection from the

other results. It appears as though wedge size does not play a role in producing results classified as outliers, as the outliers came from results on wedges of different sizes. It also seems unlikely that a specific ring would display higher deflection due to increased iodine exposure, as the iodine present sublimated into a gas that would spread evenly throughout the ampoule. It is possible that these high deflection rings received a higher strain level when being loaded onto the static wedge or featured a small mechanical defect that led to increased deflection.

#### 4.3.1.1.2 Regression with outliers excluded

After the outliers are excluded, a regression analysis performed on the revised dataset indicates that the confidence in the existence of a linear relationship between O<sub>2</sub> gas pressure and deflection improved (*i.e.*, the *p*-value decreased from 0.13 to 0.06). The regression includes an intercept of 1.1 mm, standard error of 0.01, and a *p*-value of  $9 \times 10^{-98}$ . The result for the O<sub>2</sub> gas variable was a coefficient of  $-9 \times 10^{-4}$  mm Torr<sup>-1</sup>, a standard error of  $4 \times 10^{-4}$ , and a *p*-value of 0.06.

Thus, with outliers excluded, O<sub>2</sub> gas could be accepted as a statistically significant factor at the 90% confidence level, but not at the 95% confidence level. At an O<sub>2</sub> level of 54 Torr, the regression predicts the deflection to decrease by  $0.05 \pm 0.02$  mm. This indicates that, according to regression analysis, it can be said with 90% confidence that the inclusion of O<sub>2</sub> gas has produced a low level of I-SCC mitigation.

#### 4.3.1.2 Oxygen Additive Static Loading Slot Size Measurements

A regression analysis is performed on the dataset summarized in Table 15 in an attempt to determine the possible effect of O<sub>2</sub> gas on the final slot size of Zr-4 rings exposed to corrosive I<sub>2</sub>. The regression results are displayed in Table 17.

Table 17: Regression results on final slot sizes for I-SCC tests including O<sub>2</sub> gas.

Variable	Coefficients	Standard Error	<i>p</i> -value
Wedge Size / mm mm <sup>-1</sup>	0.916	0.027	$3 \times 10^{-60}$
Temperature / mm °C <sup>-1</sup>	0.035	0.001	$1 \times 10^{-46}$
O <sub>2</sub> Gas / mm Torr <sup>-1</sup>	-0.001	0.002	0.68

These results further confirm the understanding that temperature and wedge size both have a very large effect on final slot size results, even in the presence of O<sub>2</sub> gas. However, the very high *p*-value associated with the variable of O<sub>2</sub> gas leads to the conclusion that the addition of O<sub>2</sub> gas does not lead to a statistically significant effect on the final slot size of Zr-4 slotted rings that have undergone static loading tests in a corrosive environment. The slot size results are presented for completeness. However, the final conclusions of this research are based upon deflection

measurements, as it is a more direct indicator of the level of corrosive attack experienced by a ring sample.

#### 4.4 Alkaline Metal Oxide and Alkali Earth Metal Oxide Additive Static Loading Results

The dataset used for the metal oxide additive investigation is comprised of 120 slotted rings placed on static wedges of various sizes in a hot (300 °C) and corrosive (1530 mg of I<sub>2</sub>) environment for five days with varied amounts of CaO and Na<sub>2</sub>O. Table 18 shows a summary of the experiments completed, as well as the previously collected baseline results.

**Table 18: Summary of the experimental conditions for investigating the influence of metal oxides on I-SCC of Zr-4 rings.**

Temperature / °C	Na <sub>2</sub> O / g	CaO / g	N
300 ± 10	0	0	24
300 ± 10	0.68 ± 0.02	0	16
300 ± 10	0.84 ± 0.02	0	8
300 ± 10	0	0.08 ± 0.02	24
300 ± 10	0	0.17 ± 0.02	24
300 ± 10	0	0.25 ± 0.02	24
300 ± 10	0	0.34 ± 0.02	24

This dataset is used to gain an understanding of how both of these oxides affect final deflection and slot size results in slotted rings of Zr-4.

##### 4.4.1 Alkaline Metal Oxide and Alkali Earth Metal Oxide Additive Static Loading Deflection Measurements

A regression analysis is performed to model the deflections experienced by each ring when loaded with 95 g using the results from the experiments displayed in Table 18. The variables included are: mass of Na<sub>2</sub>O powder, mass of CaO powder, and wedge size. Since temperature and iodine concentration remained the same in all experiments, these factors are not included as variables in the regression analysis. The results for each variable from the preliminary regression results are shown in Table 19.

**Table 19: Initial regression results for metal oxide additive experiments.**

Variable	Coefficients	Standard Error	<i>p</i> -value
Na <sub>2</sub> O / mm g <sup>-1</sup>	-0.22	0.03	2 x 10 <sup>-12</sup>
CaO / mm g <sup>-1</sup>	-0.82	0.06	7 x 10 <sup>-26</sup>
Wedge Size / mm mm <sup>-1</sup>	1 x 10 <sup>-3</sup>	3 x 10 <sup>-3</sup>	0.69

Negative coefficients and low *p*-values (<0.05) in Table 19 indicate that increasing amounts of Na<sub>2</sub>O or CaO mass lead to a statistically significant decrease in the slotted ring deflection induced by a 95 g mass load. Conversely, the large *p*-value (>0.05) for wedge size once again indicates that the value of wedge size (*i.e.*, induced stress) does not display a correlation with 95 g induced ring deflection. However, as these oxides have different molar masses (Na<sub>2</sub>O = 62 g mol<sup>-1</sup> and CaO = 56 g mol<sup>-1</sup>) it is difficult to compare the relative impact of these oxides on ring deflection purely based on mass (where the coefficient unit is mm g<sup>-1</sup>). Therefore, the regression is modified to determine the deflection decreases resulting from one mole of each oxide. The mass values are converted into moles using Equation 12 and Equation 13:

$$n_{Na_2O} = \frac{m_{Na_2O}}{M_{Na_2O}} \quad \text{Equation 12}$$

$$n_{CaO} = \frac{m_{CaO}}{M_{CaO}} \quad \text{Equation 13}$$

Where *n* is moles, *m* is mass, and *M* is molar mass. This conversion allows a comparison of the decrease in deflection versus moles of oxide. The results from an updated regression using mole values (with a y-intercept value of 1.06 mm, a standard error of 0.02, and a *p*-value of 4.14 x 10<sup>-81</sup>) are shown below in Table 20.

**Table 20: Final regression statistics on deflection results where moles of metal oxides are the inputs.**

Variable	Coefficients / mm mole <sup>-1</sup>	Standard Error	<i>p</i> -value
Na <sub>2</sub> O	-14	2	2 x 10 <sup>-12</sup>
CaO	-46	4	4 x 10 <sup>-26</sup>

It can be seen that both of the *p*-values are quite low, suggesting that the effect of both oxides are statistically significant. From the negative slopes in Table 20 it can be stated that including small amounts of CaO results in approximately three times less corrosion in samples than from including small amounts of Na<sub>2</sub>O. It should be

noted that the regression analysis used to perform this investigation presupposes that the factors being analyzed follow a linear trend. Figure 22 and Figure 23 display the results from the experiments in an attempt to determine whether the assumption of linearity holds true for the dataset.

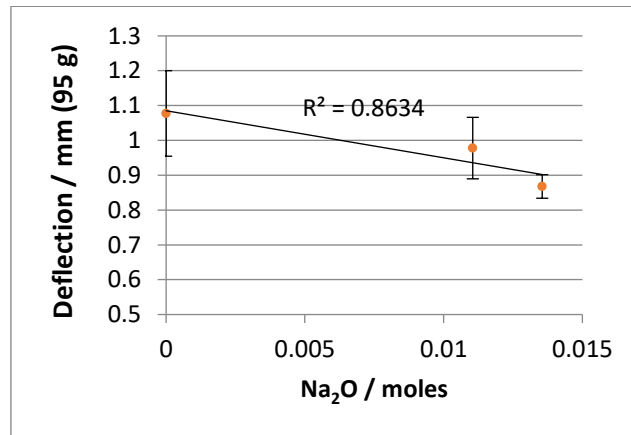


Figure 22: Average Na<sub>2</sub>O deflection results (error bars = 1 standard deviation).

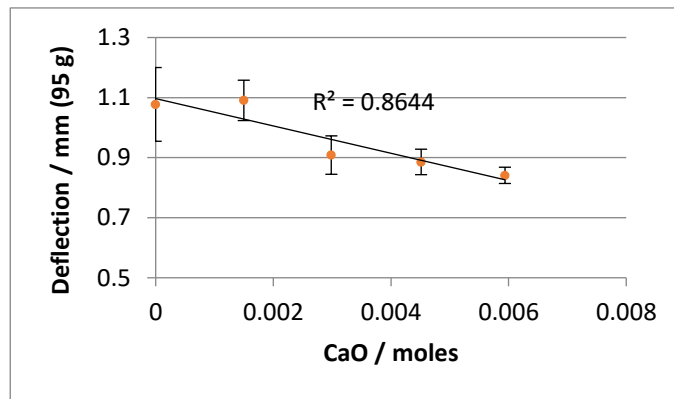


Figure 23: Average CaO deflection results (error bars = 1 standard deviation).

Although the Na<sub>2</sub>O trend line correlates well with the experimental data ( $R^2 > 0.85$ ), having only three  $x$ -values is likely insufficient to conclusively state a linear relationship (Figure 22). Consequently, experimental efforts are undertaken to include varying levels of CaO in order to clarify whether the correlation between oxide levels and deflection is linear. In Figure 23 there is a reasonably strong negative linear correlation ( $R^2 > 0.85$ ) seen in the range of CaO results displayed, which features a more varied set of oxide levels. Although the current results are

preliminary, the decreasing trend in ring deflection suggests that these oxides may assist in I-SCC mitigation.

These results were presented in a conference paper [58], after which the investigation was continued by Ferrier *et al.*, [38] and [59]. Ref [57] includes a set of experiments where MgO is also analyzed as an additive. The author of this thesis is also a co-author of these peer-reviewed journals and present select results from Ref [57] in this thesis. MgO results are not included in the research, which is why the regression analysis results in Table 20 do not match exactly with the corresponding results presented by Ferrier *et al.* The results presented in Section 4.5 are also from the Ferrier *et al.*, [38] and are included for completeness and to assist the discussion in Chapter 5.

#### 4.4.2 Alkaline Metal Oxide and Alkali Earth Metal Oxide Additive Static Loading Slot Size Measurements

A regression analysis is performed to examine how the inclusion of CaO and Na<sub>2</sub>O affect the final slot size of Zr-4 rings placed on static wedges in a hot, corrosive environment. The temperature and amount of I<sub>2</sub> included are constant for every experiment in question, and as such are not included as variables in the regression. Table 21 shows the results from the regression.

**Table 21: Results from regression analysis on the effect of CaO and Na<sub>2</sub>O on the final slot size of Zr-4 rings that have undergone I-SCC experiments.**

Variable	Coefficient	Standard Error	<i>p</i> -value
Wedge Size / mm	0.81	0.02	2 x 10 <sup>-73</sup>
Na <sub>2</sub> O / g	-0.17	0.21	0.42
CaO / g	-0.23	0.47	0.62

Wedge size continues to show a large, reliable effect on the final slot size of statically loaded Zr-4 rings (*p*-value << 0.05). CaO and Na<sub>2</sub>O both do not appear to have any effect on the final slot size of the rings, as both have very large *p*-values (Table 21). From these results it can be concluded that while both CaO and Na<sub>2</sub>O have been shown to cause reduction in deflection results, neither oxide has shown an ability to influence the final slot size of the slotted rings in question. Again, deflection measurements are used to draw final conclusions, as it is more indicative of the level of corrosion experienced by a sample.

### 4.5 Protective Coating Static Loading Results

While CANLUB has been proven to be effective, it was originally developed as a mechanical lubricant. If an SCC mitigation strategy were developed with the ability for impurities to sequester I<sub>2</sub> in mind, it could lead to a significant improvement in the overall performance of the coating. The potential benefits from improving the SCC mitigation coating utilized in reactors could help CANDU reactors safely

develop more advanced fuel cycles (*i.e.*, higher burnups, load following, *etc.*) and reach higher levels of reactor performance. This could be achieved by looking to a new coating that features higher levels of impurities.

Pyromark features higher concentrations of several different alkaline metals and alkali metal oxides [38]. This includes Ca and Na, the two metals used for the metal oxide experiments that displayed I-SCC mitigation abilities. Although K and Ba were not experimentally investigated it is believed that they may also sequester I<sub>2</sub> as they all behave chemically like Na and Ca. The results from experiments with MgO by Ferrier *et al.*, confirmed the hypothesized protective properties of the additive, similar to the Ca and Na results in this thesis. Table 4 lists the concentrations of Mg, Ca, and Na within CANLUB and Pyromark determined using ICPMS.

The paper from Ferrier *et al.*, [38] describes static loading tests on rings coated with Pyromark, using the same procedure explained in this thesis (Section 3.4). Section 1.9.1 describes the work performed by the different authors working on the RMC I-SCC mitigation program. The 45 g mass load deflections are summarized in Table 22.

**Table 22: 45 g deflections for uncoated, CANLUB coated, and Pyromark coated rings; adapted from [59].**

Coating	Iodine Mass / mg	45 g Deflection / mm
Uncoated	1800 ± 10	0.53 ± 0.05
CANLUB	1800 ± 10	0.54 ± 0.03
Pyromark	1800 ± 10	0.41 ± 0.03

There does not appear to be any distinction between uncoated rings and CANLUB coated rings in terms of deflections when exposed to 1800 mg of I<sub>2</sub>. However, Pyromark coated rings show a significant decrease in ring deflection results. This evidence points towards the possibility Pyromark being more effective at mitigating I-SCC when high concentrations of I<sub>2</sub> are present in the absence of radiation. The ability of Pyromark to improve deflections is likely a direct result of the ability to sequester I<sub>2</sub> from interacting with Zr-4, which, given the effect of Na<sub>2</sub>O and CaO, is likely due to the high level of metal impurities present in Pyromark when compared to CANLUB.

Experiments were also performed by Ferrier *et al.*, where the CANLUB coating was doped with higher concentrations of Na, Ca, and Mg [38]. These additives were introduced into CANLUB in amounts that recreated the levels of impurities present in the Pyromark coating. However, these rings samples did not provide any I-SCC mitigation, much like in the non-doped CANLUB experiments (Table 23). It was noted by Ferrier *et al.*, [38] that there is a significant reduction in the mechanical

integrity of CANLUB layer in experiments. This could explain why there is no I-SCC mitigation seen in any of the CANLUB experiments, an idea that is explored further in the following analysis and discussion section.

**Table 23: 95 g deflections for uncoated, doped CANLUB coated; adapted from [59].**

<b>Coating</b>	<b>Added Elements</b>	<b>Iodine Mass / mg</b>	<b>95 g Deflection / mm</b>
Pyromark	N/A	$1800 \pm 10$	$0.8 \pm 0.1$
Uncoated	N/A	$1800 \pm 10$	$1.0 \pm 0.1$
Undoped CANLUB	N/A	$1800 \pm 10$	$1.2 \pm 0.1$
Doped CANLUB	Na	$1800 \pm 10$	$1.4 \pm 0.2$
Doped CANLUB	Ca	$1800 \pm 10$	$1.4 \pm 0.1$
Doped CANLUB	Mg	$1800 \pm 10$	$1.3 \pm 0.1$
Doped CANLUB	Na, Ca, and Mg	$1800 \pm 10$	$1.3 \pm 0.2$

## 5 Discussion

This section analyzes the experimental results.

### 5.1 I-SCC Bare Ring Experiments

Deflections from bare Zr-4 slotted rings display a strong dependency on the amount of  $I_2$  present within the ampoules. Deflections are used to record small changes in the thickness of the rings, as caused by an attack of  $I_2$  on the surface. The process of  $I_2$  actively attacking Zr-4 is detailed in Section 3.5.

If there is truly a surface attack being experienced by the rings, it should be noticeable under visual inspection. Figure 16 displays SEM images of a Zr-4 surface before and after corrosion testing.

Figure 16A displays the surface of bare Zr-4 before being exposed to a corrosive environment. Figure 16B, which displays the surface of a bare Zr-4 statically loaded and placed within a hot and corrosive environment, shows lighter areas across the surface of the Zr-4. This is believed to be the corrosion that leads to the changes seen in deflection measurements. As  $I_2$  interacts with Zr-4 it actively removes Zr molecules from the surface, creating a reduction in the thickness of the material, which manifests as lighter regions in the SEM images. This confirms that the changes in deflections analyzed are due to the hypothesized corrosive process (Section 1.5.2). This also leads one to believe that the I-SCC mitigation strategies that reduce deflections were likely succeeding by preventing this process from occurring.

### 5.2 Comparison with Previous Work Investigating $O_2$ Additions

The relationship between  $O_2$  gas pressure and mechanical deflection is not an obviously linear one, and previous work suggests that the relationship should not be linear. For example, Une *et al.*, [30] found that SCC mitigation occurred in Zircaloy-2 (Zr-2) when the oxygen pressure exceeded a threshold value (*i.e.*, 28 Torr at 300 °C), and that increasing the oxygen gas pressure above the threshold led only to marginal improvements. Evidence of SCC mitigation has also been observed by Une *et al.*, in Zr-4 when the  $O_2$  gas pressure surpassed a threshold pressure of approximately 11.75 Torr at 300 °C, albeit in small sample sizes [29]. The differences in the  $O_2$  pressure thresholds seen by Une *et al.*, and what was observed in experiments described in this research may arise from the fact that Une *et al.* investigated the time required for Zr-2 to reach the failure regime, while this research analyses pre-failure corrosion levels in Zr-4 samples.

Figure 21 (with outliers removed) shows that a relationship may exist whereby a threshold oxygen pressure is reached and limited improvements in deflection are

observed above the threshold pressure. For instance, if the deflections corresponding to 6, 12, and 54 Torr (all pressures at room temperature) are not distinct from one another, yet significantly lower than the deflection corresponding to the baseline condition (0 Torr added), then the non-linear trend can be characterized by a plateau region covering all pressures above a threshold pressure of 6 Torr (approximately 11.75 Torr at 300 °C).

To determine quantitatively whether this trend is occurring, a *two-tailed*, type-three *t*-test [64, 67] was performed. Oxygen data was split into two arrays: deflection results where O<sub>2</sub> gas was introduced and deflection results where O<sub>2</sub> gas was not introduced (baseline results). The reason that the *t*-test produced a higher confidence level than the regression results lies within the fact that regression analysis presupposes a linear relationship across two variables. If these data were truly experiencing a plateau after the first point, there would be no linear relationship to be found across the three levels of O<sub>2</sub> gas tested. This would lead to a low R<sup>2</sup> value (Figure 21) and a high *p*-value (Table 16). The *t*-test analysis, however, simply states the likelihood that two datasets are distinct and thus was able to provide an understanding at a higher confidence level. This analysis indicates that Figure 21 likely illustrates a non-linear relationship between O<sub>2</sub> gas pressure and mechanical deflection characterized by a plateau region covering all pressures above a threshold pressure of 6 Torr (approximately 11.75 Torr at 300 °C). The *t*-test returned a result of 0.0165; meaning that it can be stated at the 95% confidence level that results with elevated O<sub>2</sub> gas were statistically distinct from the baseline results.

### 5.3 Feasibility of Metal Oxide Additives

One of the main caveats that should be noted for the Na<sub>2</sub>O and CaO additives results in this research is that the additives are introduced into the ampoules as a powder, as opposed to being applied directly to the rings *via* a coating applied to the sheath surface.

Caveats aside, the observations described in Section 4 are promising in terms of the potential SCC mitigation properties of Na<sub>2</sub>O and CaO, as both were shown to be able to significantly reduce the corrosive attack of I<sub>2</sub> on Zr-4 when introduced into the tests in small amounts.

The ability of metal oxides such as Na<sub>2</sub>O and CaO to successfully sequester I<sub>2</sub> is only the first step in proving the feasibility of introducing these oxides into CANLUB in order to improve SCC mitigation. To further assess the feasibility of these additives, the actual amount of each oxide that would be required to successfully mitigate I-SCC needs to be determined. It then would need to be shown that these levels of additives would not cause significant effects to the neutron economy of the reactor, and not introduce harmful isotopes into the reactor through neutron activation.

From the deflections described in Section 4.4 it appears that additive amounts of 0.84 g<sub>Na2O</sub> and 0.34 g<sub>CaO</sub> are able to fully mitigate the effect of 1530 mg of I<sub>2</sub> (16 mg<sub>I2</sub>·cm<sup>-3</sup>). The calculations focus on amount of metals, as opposed to amount of metal oxides, as there is a higher confidence in the effect of the metals when compared to the confidence in the effect of the oxygen molecules, based on the work in this thesis. The mass contributions of metal from the 0.84 g<sub>Na2O</sub> and 0.34 g<sub>CaO</sub> amounts are 0.62 g<sub>Na</sub> and 0.23 g<sub>Ca</sub>.

Thus, to fully neutralize the effects of an environment with 16 mg<sub>I2</sub>·cm<sup>-3</sup> (corresponds to the concentration of 1530 mg of I<sub>2</sub> used in many experiments of this research), on Zr-4 sheathing of ~40 mm in length, 0.23 g<sub>Ca</sub> or 0.62 g<sub>Na</sub> were required. These are very high values when one considers that the total amount of CANLUB present in an ampoule with eight coated rings is approximately 0.06 g. However, within the metal oxide additive experiments, the I<sub>2</sub> concentration is 16 mg·cm<sub>I2</sub><sup>-3</sup>, while the accepted range of I<sub>2</sub> concentration near the sheath during reactor operation is 1 mg·cm<sub>I2</sub><sup>-3</sup>[28,68] (*i.e.*, this is the current concentration of I<sub>2</sub> produced from fission products and radiolysis addressed using the current I-SCC mitigation strategies in operating CANDU reactors). Thus, the levels of I<sub>2</sub> experienced within the experiment ampoules in this research are significantly higher than what is experienced even at extended burnup. From this, one can assume that the amount of oxide required in reactors would be much lower than the values determined from deflection experiments.

Additionally, it must be considered that there is more than a single impurity present within CANLUB. The large value for the required mass of an oxide to mitigate the effect of I<sub>2</sub> seems quite high, as it is being asked to carry the entire load of I-SCC mitigation. So, while 0.01 g<sub>Ca</sub>, and 0.04 g<sub>Na</sub> would be necessary to have a mitigating effect in an environment of 1 mg·cm<sub>I2</sub><sup>-3</sup> these estimations were made from experiments of oxides in isolation (values determined by dividing 0.62 g<sub>Na</sub> and 0.23 g<sub>Ca</sub> by 16, as those values were determined for 16 mg<sub>I2</sub>·cm<sup>-3</sup>, linearity for this relationship is established through Figure 24). It is expected that the other metal impurities present in CANLUB may be able bear some of the I<sub>2</sub> sequestering load; thereby lowering the amounts of metal oxide additions that may be required.

The concentration of I<sub>2</sub> that is expected at the sheath under extended burnup is a useful piece of information for further experiments on metal oxide additives. As the production of I<sub>2</sub> appears to follow a linear trend, one could extrapolate the relationship between burnup and the amount of I<sub>2</sub> to create a rough estimation of the amount of I<sub>2</sub> that would be produced at extended burnup. Figure 24 plots the values from Table 2 to develop an expression for I<sub>2</sub> production as a function of burnup.

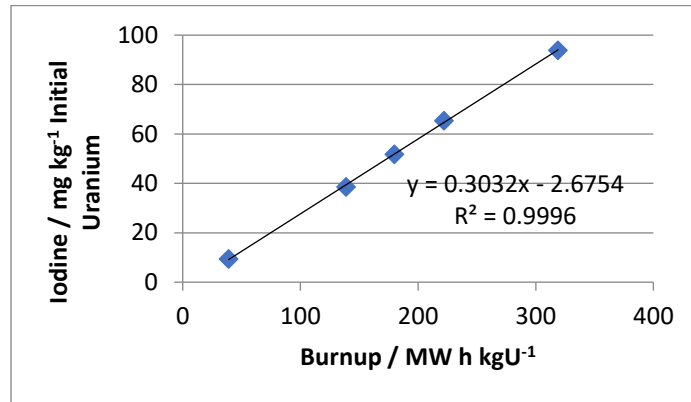


Figure 24: Relationship between I<sub>2</sub> production and burnup, adapted from Table 2.

From the relationship displayed in Figure 24 one can create a rough estimation of the amount of I<sub>2</sub> that would be produced at extended burnups by assuming continued linearity in the relationship between burnup and I<sub>2</sub> production. For example, if the burnup in the reactor was increased from 320 MW h kgU<sup>-1</sup> to 625 MW h kgU<sup>-1</sup> the amount of I<sub>2</sub> produced for every kg of uranium would approximately double. From this, one could determine how much of this I<sub>2</sub> would be able to reach the pellet-cladding gap. It seems logical that I<sub>2</sub> would diffuse through the fuel into the pellet-cladding gap at a similar rate to what is seen at standard burnup. This means that if burnup was increased from 320 MW h kgU<sup>-1</sup> to 625 MW h kgU<sup>-1</sup> the concentration of I<sub>2</sub> present at the sheath would also double, which produces an I<sub>2</sub> concentration of 2 mg<sub>I<sub>2</sub></sub> cm<sup>-3</sup>. This concentration is still significantly lower than what was experienced by the rings tested in this research. It should be noted that the burnup of 625 MW h kgU<sup>-1</sup> is almost entirely arbitrary; the actual level of extended burnup may be significantly different. Also, these are rudimentary calculations to develop an approximate value for an expected concentration of I<sub>2</sub> at extended burnup. Thus, it would not be sufficient to state that successful mitigation at 2 mg<sub>I<sub>2</sub></sub> cm<sup>-3</sup> would cover all levels of I<sub>2</sub> that would be experienced at extended burnup. This is especially true when one considers that to be fully commissioned it would need to be shown that SCC mitigation would occur beyond standard operation. However, the rudimentary calculations for the amount of additive required are much less for 2 mg<sub>I<sub>2</sub></sub> cm<sup>-3</sup> with ~ 0.03 g<sub>Ca</sub> and ~0.08 g<sub>Na</sub> required for a single fuel sheathing.

The following subsection discusses the two coatings, CANLUB and Pyromark, in relation to I-SCC mitigation.

## 5.4 Coatings

CANLUB has been found to not improve deflections in any noticeable fashion, which may seem like an unlikely conclusion, as CANLUB has been shown to be

very effective at preventing SCC failures in reactors (Section 1.6.2). While the concentration of  $I_2$  within the experiments detailed in this section range from 16-19  $mg_{I_2} \cdot cm^{-3}$ , the  $I_2$  concentration within a CANDU reactor is accepted as 1  $mg_{I_2} \cdot cm^{-3}$  near the sheath [28,69]. The high concentrations of  $I_2$  are required for the experiments, as it would take much longer than five days to see appreciable levels of corrosion in rings exposed to in-reactor levels of  $I_2$ . So, while CANLUB is effective at the lower concentrations of  $I_2$ , it struggles at higher concentrations, as it was not designed to experience these elevated levels of corrosive elements. In fact, this helps show that if CANDU reactors were ever to utilize higher fuel burnups (which would create increased fission product release) there may be a need to improve upon CANLUB in order to protect the sheath from SCC failures.

While the concentrations of  $I_2$  introduced by the experiments are too high for CANLUB to be effective, small amounts of CaO and Na<sub>2</sub>O are able to reduce the corrosive attacks experienced by ring samples (Section 4.4). This supports the theory that the impurities within CANLUB are responsible for its SCC mitigation properties. The experiments that were performed on rings coated with doped CANLUB to represent the level of impurities similar to what is seen in Pyromark. Table 23 showed that the rings coated with doped CANLUB had no tangible I-SCC mitigation. This is in contrast to the significant I-SCC mitigation in samples coated in Pyromark (Table 22). These results cast doubt on the potential strategy to dope CANLUB with additional impurities to further improve performance when the commercially available coating Pyromark is providing more I-SCC mitigation in all experiments to date.

It is unclear why the experiments with doped CANLUB are not able to re-create the I-SCC mitigation results seen from additives in the experiments of this research. As the additives are applied directly to the rings it may have led to more corrosive  $I_2$  being present near the samples. It is also noted by Ferrier *et. al.*, [56] that increasing the level of impurities within the coating may have had some detrimental effects on the mechanical performance of the coating.

While Pyromark continues to perform well in experiments at RMC, it is desirable to continue to investigate the root causes of the I-SCC mitigation while continuing research into the feasibility of Pyromark.

## **5.5 Potential Effects of Radiation on Metal Oxide Additives**

The experiments performed in this research were completed entirely in the absence of radiation. It is important to consider how any elements introduced into the reactor would respond to the presence of radiation and neutron bombardment. The generally accepted flux of a CANDU reactor in standard operation is  $1 \cdot 10^{14} \text{ n} \cdot \text{cm}^{-2} \cdot \text{s}^{-1}$  with

neutron energies ranging between  $2.5 \cdot 10^{-3}$ - $4.4 \cdot 10^{-1}$  MeV, in the range of thermal neutrons [70]. This rate was used with the National Institute of Standards and Technology Center for Neutron Research tool for Neutron Activation and Scattering Calculation [71], a tool that performs calculations to determine the isotopes that theoretically should be produced from neutron activation of Na or Ca (a thermal/fast neutron flux of 0.5 is assumed). The calculations are based on 0.01 g<sub>Ca</sub> and 0.04 g<sub>Na</sub>, (the calculated amounts required per sheathing, described in Section 5.3) being exposed to these flux conditions for one year. Natural isotopic abundances are used for the calculations. Notable results are shown in Table 24 and Table 25.

**Table 24: Notable products of neutron activation of 0.01 g<sub>Ca</sub> exposed to flux levels of CANDU reactors for 1 year, adapted from calculations by [71].**

Element	Reaction	Product	Half-Life	Activity / $\mu$ Ci
Ca-40	Neutron Activation	Ca-41	103,000 years	$1.12 \cdot 10^3$
Ca-44	Neutron Activation	Ca-45	165 days	3.8
Ca-40	Neutron Decay	Ar-37	34.8 days	$8.6 \cdot 10^{-1}$

**Table 25: Notable products of neutron activation of 0.04 g<sub>Na</sub> exposed to flux levels of CANDU reactors for 1 year, adapted from calculations by [71].**

Element	Reaction	Product	Half-Life	Activity / $\mu$ Ci
Na-23	Neutron Decay	Na-22	2.6 years	2.2
Na-24	Neutron Activation	Ca-45	165 days	0

If a failure occurs in the sheath, it allows the transport of fission products through the coolant, and if metal oxide additives are introduced as a mitigation strategy to the fuel-sheath interface, they would also be able to enter the PHT system if a failure occurred. The majority of compounds formed with Ca or Na are water soluble, meaning that once Na or Ca enter the coolant they would most likely be transferred by the coolant flow. Table 24 and Table 25 list the products of note if 0.01 g<sub>Ca</sub> and 0.04 g<sub>Na</sub> were exposed to CANDU reactor fluxes for a year. The most notable activation product with the highest reported activity in Table 24 and Table 25 is Ca-41, which has a half-life of 103,000 years and would still be providing about 1 mCi of activity after a year of neutron bombardment in the reactor. Na-23 (half-life of 2.6 years) is also a product of note, as it would still be providing 2.2  $\mu$ Ci of activity after a year of neutron bombardment. These safety concerns would not be taken lightly, and there would need to be assurance that these particles would not be transported throughout the NPP if a sheath failure were to occur. However, the bulk of these concerns would be addressed if it were shown that the amount of additives required is small enough that they become negligible when compared to the larger volume of coolant in the PHT of a NPP.

Calculations in Section 5.3 estimated that, for a single sheathing, 0.01 g<sub>Ca</sub> and 0.04 g<sub>Na</sub> would be necessary to have a mitigating effect in an environment of 1 mg<sub>I<sub>2</sub></sub>·cm<sup>-3</sup>, the accepted I<sub>2</sub> concentration experienced by CANLUB coated sheaths in current reactor operation. The CANDU PHT system contains approximately 192,000 L of heavy water [72]. The density of heavy water is 1.107 g cm<sup>-3</sup> at 298.15 K [73] meaning there is approximately 212,544 kg of heavy water in the PHT system. If a single sheath failure were to occur where .01 g<sub>Ca</sub> and 0.04 g<sub>Na</sub> were to fully enter the main PHT system, mass percentages of the impurities for the PHT system would be 4.7·10<sup>-11</sup> g<sub>Ca</sub>·g<sub>D<sub>2</sub>O</sub><sup>-1</sup> and 1.9·10<sup>-10</sup> g<sub>Na</sub>·g<sub>D<sub>2</sub>O</sub><sup>-1</sup>. Studies investigating particulates in the PHT system by Burrill and Balakrishnan calculated an overall particulate concentration of 1.3·10<sup>-3</sup> mg·Kg<sub>D<sub>2</sub>O</sub><sup>-1</sup> [74], orders of magnitude lower than the overall level of impurities seen in the PHT system. This shows that the amount of impurities that would be introduced into the PHT system if a sheathing doped with additives were to fail would be negligible and that the amount of impurities present would need to increase significantly before their potential contributions could be seen as significant within the overall level of impurities present in the PHT system.

The effect on the neutron economy of the reactor caused by neutron absorptions in Na and Ca is another factor that must be considered. If the additives absorb a large percentage of available neutrons it would impact the number of fissions the reactor could produce. Based on the mass percentages calculated above, this would seem to be a minor concern.

Another study on the feasibility of metal oxide additives that would have to be performed prior to practical use is on how these oxides would affect the mechanical properties of CANLUB. It would need to be shown that the amounts of oxide required would not be detrimental to the original coating in any significant way. This process could be very similar to the mechanical tests performed by Ferrier *et al.*, [59] where it is noticed that there might be degradation to the coating.

## 6 Conclusions

The following conclusions are based on experiments completed for this research or reported in papers co-authored by the author of this thesis [38,58, 59].

- A strong, positive relationship is established between the amount of corrosive attack experienced by ring samples (*i.e.*, increased deflections) and the amount of iodine included in the experiment. The large, reliable effect on deflection results from iodine inclusion forms the baseline for I-SCC that mitigation strategies are evaluated against.
- Temperatures and strain level (*i.e.* wedge size) are also investigated as variables in I-SCC on the slotted ring samples. Temperature is shown to have a small, unreliable effect on deflection results. Varying the width of the wedge is shown to have no effect on deflection results. As such, wedge size is varied freely in subsequent experiments while temperature is largely held constant outside of exploring for certain interaction effects.
- It is shown at a 90% confidence level that the inclusion of O<sub>2</sub> gas provides a low-level protection from I-SCC.
- Significant reductions in I-SCC induced corrosion are seen in ring samples that are tested with varying levels of Na<sub>2</sub>O and CaO in the experiments. There is a large and reliable decrease in corrosive attack experienced by rings with additives included in the experiments.
- Rings coated with Pyromark display significant levels of I-SCC mitigation. In contrast, rings coated with CANLUB display no significant I-SCC mitigation for high levels of I<sub>2</sub> exposure. Further, rings tested that had been coated with CANLUB doped with the metal oxide additives show no I-SCC mitigation for high levels of I<sub>2</sub> exposure. Based on these results, Pyromark is a coating worth evaluating further.

This work has been completed as part of a larger effort to investigate the phenomenon of I-SCC in CANDU reactors, both at RMC and within the larger industry [1,2,38,56,57,58]. A repeatable experimental procedure has been developed wherein statically loaded rings are used to evaluate the potential for I-SCC mitigation strategies. This can be done using the baseline for the corrosive effects established in this research (note this procedure was developed based on the work of Wood and Quastel *et al.*, [1,56]). The motivation for investigating I-SCC mitigation strategies is based on improving the performance (in terms of economics) of existing and potential future CANDU reactors by allowing more aggressive fuelling schedules (*i.e.*, extended burnup or load following). The work in this thesis has shown that O<sub>2</sub>

gas may have some I-SCC mitigation properties, and that  $\text{Na}_2\text{O}$  and  $\text{CaO}$  both have the ability to reduce the impact of I-SCC. These results can be used moving forward in the ongoing effort to further comprehend I-SCC. Further, the procedure developed in this research has been used in continued experiments that have helped to identify one of the more promising commercial options, Pyromark [38,57], and has been the basis for three published papers [38, 57, 58]§.

---

§ The author of this thesis is the main author of Ref. [59] and a co-author of the two peer-reviewed journal papers [38], [57].

## 7 Future Recommendations

This section proposes future experiments and investigations that would advance the understandings of I-SCC and potential mitigation strategies.

### 7.1 Further Investigation into O<sub>2</sub> Gas Additions

The desired interaction of O<sub>2</sub> gas introduced into the ampoules was to be available to re-form the protective oxide layer on the bare Zr-4 rings. The experiments that explored the mitigation properties of O<sub>2</sub> with respect to I-SCC showed that there is likely some mitigation being provided by the presence of the gas. However, the experiments at either 12 or 54 Torr did not show any higher level of mitigation than the experiments performed at 6 Torr. It is theorized by Une *et. al.*, [29] that potentially there is a threshold amount of oxygen available where some mitigation is provided, but no further mitigation is achieved from introducing excess oxygen. A t-test performed on the results with and without oxygen included showed that the two datasets are different from one another at a statistically significant level.

If there is a threshold of O<sub>2</sub> gas where I-SCC mitigation is achieved *and* maximized it would be desirable to determine this threshold. Further, it is unknown what the relationship between O<sub>2</sub> gas and I-SCC mitigation is below the hypothesized threshold. Thus, an experiment is proposed to utilize the same experimental method described in this research to investigate lower levels of O<sub>2</sub> gas. The experiments would be below the 6 Torr amount to determine the threshold amount of O<sub>2</sub> gas. Then, experiments would be performed with even less O<sub>2</sub> gas to understand the relationship prior to the threshold.

### 7.2 Further Investigation into Oxide Additives

An experiment could be performed that would prove useful in investigating the feasibility of metal oxide additives in CANLUB by providing insight into the actual amount of each oxide that would be required to provide the desired levels of SCC mitigation. The experiment would follow roughly the same procedure as the experiments performed in this research, where slotted rings are statically loaded and heated in an ampoule with corrosive I<sub>2</sub> present. The amount of I<sub>2</sub> introduced must be set to where CANLUB has been shown to be ineffective, but still within a reasonable estimate of what could be expected at extended burnup in a CANDU reactor (potentially 2-10 mg<sub>I<sub>2</sub></sub>·cm<sup>-3</sup>, see Section 5.3 for detailed discussion on I<sub>2</sub> concentrations at regular and extended burnups). The rings would be coated with a mixture of CANLUB and small amounts of Na<sub>2</sub>O, CaO, or both. This process could be repeated across a large range of values for the amounts of oxide included. From these experiments one could determine the amount of oxide that was required for I-SCC mitigation at a specific level of I<sub>2</sub> concentration in conjunction with the supposed I-SCC mitigation effects of CANLUB. This would provide a more realistic prediction about the levels of Na<sub>2</sub>O or CaO that would be required to provide I-SCC mitigation at extended burnup alongside CANLUB.

### **7.3 Further Pyromark Testing**

Pyromark has been shown to contain impurities believed to be driving I-SCC mitigation [56]. Further, Pyromark performed well in the static loading tests presented in this research from the work of Ferrier *et al.*, [58,38]. Based on these observations, if the goal is to work towards a coating solution that could be used in operating CANDU reactors, further research into Pyromark seems warranted. The following recommended experiments should all be performed on slotted ring samples coated with Pyromark to further evaluate the coating's potential as part of an improved I-SCC mitigation strategy.

### **7.4 Irradiation Testing**

Before any I-SCC mitigation strategy can be considered for practical application, it must undergo testing that includes radiation fields to mimic the conditions experienced by fuel sheathings in commercial CANDU operation. The concerns related to the effects of radiation on the additives are explained in Section 5.5. Thus, any I-SCC mitigation slotted ring experiments that include radiation fields should include an assessment of whether any harmful or undesirable isotopes are produced during the experiment.

Further, hypothesized radiolysis of CsI causing dissociation of the molecule to release free iodine and is believed to be paramount in I-SCC. Thus, irradiation experiments would further investigate the importance of radiolysis in I-SCC. The strength of the radiation field present and the amount of iodine could be varied in order to develop a relationship of I-SCC. Experiments could include Cs, allowing the CsI molecule to form to ensure the radiolysis that is hypothesized as the process for creating freely available I<sub>2</sub> behaves as expected. This would provide further insights into the mechanism of I-SCC in CANDU fuel sheathings.

### **7.5 Advanced Fuel Cycles and Dynamic Loading**

Another aspect of developing advanced fuel cycles that needs to be considered is the changes in the dynamic loading that the sheath would experience. This could mean exposing the rings to larger dynamic loads when moving to higher burnups. However, advanced fuel cycles could also include load following, which could involve reactors responding to the requirements of the grid or introducing a power ramping schedule to the reactors. In either situation it would lead to a significant increase in the number of power ramps experienced by the sheathing in-reactor.

There has been limited experimental research investigating the effects of cyclical loading on I-SCC in CANDU fuel sheathings, with the work of Tayal *et al.*, providing the majority of the research from small sample size experiments in commercial reactors [33,39]. If an apparatus could be designed that recreates the conditions in this experiment (*i.e.* an evacuated ampoule at high temperatures and controlled amount of iodine present), but allows for the strain level (*i.e.*, wedge size)

to be oscillated, it would potentially provide insights into the effects of heavy loading on these samples. Strain levels could be derived to represent the strain levels experienced by sheaths in a typical load following manoeuvre and repeated numerous times to mimic the life of a fuel sheathing in a reactor performing regular load following. It would also be prudent to design this apparatus in such a way that allows for irradiation testing, as it would allow for factors of interest to be tested in parallel with the factors discussed in the previous subsection that also warrant further investigation.

## 8 References

- [1] J.C. Wood, “Factors affecting stress corrosion cracking of zircaloy in iodine vapour”, *Journal of Nuclear Materials*, vol. 45, no. 2, pp. 105–122, 1972.
- [2] B.J. Lewis, W.T. Thompson, M.R. Kleczek, K. Shaheen, M. Juhas, F.C. Iglesias, “Modelling of iodine-induced stress corrosion cracking in CANDU fuel”, *Journal of Nuclear Materials*, vol. 408, no. 3, pp. 209-223, 2011.
- [3] How Reactors Work, *Canadian Nuclear Association*, Available at: <https://cna.ca/technology/energy/how-reactors-work/>, Accessed on: November 10, 2018.
- [4] R. Chaplin, *The Essential CANDU, A Textbook on the CANDU Nuclear Power Plant Technology*, Editor-in-Chief Wm. J. Garland, Chapter 1, *University Network of Excellence in Nuclear Engineering (UNENE)*, ISBN 0-9730040. Retrieved from <https://www.unene.ca/education/candu-textbook> on July 30, 2018.
- [5] Kaye & Laby Tables of Physical & Chemical Constants, *National Physical Library*, Chapter 4.7, Available at: <http://www.kayelaby.npl.co.uk/toc/>, Accessed on: November 2, 2018.
- [6] Nuclear Fission: Basics, *atomicarchive.com*, Available at: <http://www.atomicarchive.com/Fission/Fission1.shtml>, Accessed on: September 23, 2018.
- [7] N.J. Carron, “An introduction to the passage of energetic particles through matter”, *CRC Press*, 2006.
- [8] J. Kopecky, J. Ch. Sublet, J.A. Simpson, R.A. Forrest, D. Nierop, “Atlas of Neutron Capture Cross Sections”, *International Atomic Energy Association*, 1997.
- [9] What is criticality?, *MIT NSE Nuclear Information Hub*, Available at: <https://mitnse.com/2011/03/18/what-is-criticality/>, Accessed on: September 23rd, 2018.
- [10] L. Clegg and J. Coady, “Radioactive decay properties of CANDU fuel”, *Atomic Energy of Canada Limited*, no. AECL--4436/2, 1977.
- [11] What is Uranium? How Does it Work?, *World Nuclear Association*, Available at: <http://www.world-nuclear.org/information-library/nuclear-fuel-cycle/introduction/what-is-uranium-how-does-it-work.aspx>, Updated Jan. 2017, Accessed on: August 3rd, 2018.
- [12] Physics of Uranium and Nuclear Energy, *World Nuclear Association*, Available at: <http://www.world-nuclear.org/information-library/nuclear-fuel-cycle/introduction/physics-of-nuclear-energy.aspx>, Accessed on: August 7, 2018.

- [13] Nuclear Data Center, Maxwellian-Averaged Cross Sections (MACS), *Japan Atomic Energy Agency*, Available at: <https://www.ndc.jaea.go.jp/nucldata/MACS/>, Accessed on: August 3, 2018.
- [14] J.A.L. Robertson, “Nuclear Energy in Canada: the CANDU System”, *Atomic Energy of Canada Limited*, no. AECL-6328, 1979.
- [15] N.K. Popov, *The Essential CANDU, A Textbook on the CANDU Nuclear Power Plant Technology*, Editor-in-Chief Wm. J. Garland, Chapter 6, *University Network of Excellence in Nuclear Engineering (UNENE)*, ISBN 0-9730040. Available at: <https://www.unene.ca/education/candu-textbook>, Accessed on: August 6, 2018.
- [16] J. Whitlock, *Canadian Nuclear FAQ*, Available at: <http://www.nuclearfaq.ca>, Accessed on August 7, 2018.
- [17] CANDU Technology, *Canadian Nuclear Association*, Available at: <https://cna.ca/technology/energy/candu-technology/>, Accessed on: August 7, 2018.
- [18] M. Tayal, “Modelling CANDU fuel under normal operating conditions”, *Atomic Energy of Canada Limited*, no. AECL--9331, 1987.
- [19] J. Montin, M.R. Floyd, Z. He and E. Kohn, “Performance of Two CANDU-6 Fuel Bundles Containing CANLUB and Non-CANLUB Production Elements”, in 7<sup>th</sup> *International Conference on CANDU Fuel*, Kingston, 2001.
- [20] N. Marchal, C. Campos, and C. Garnier, “Finite element simulation of Pellet-Cladding Interaction (PCI) in nuclear fuel rods”, *Computational Materials Science*, vol. 45, no. 3, pp. 821–826, 2009.
- [21] D.R. Olander, “Nuclear Fuels: Present and Future”, *Engineering Journal*, vol. 13, no. 1, pp. 1–28, 2009.
- [22] H.E. Rosinger, “A model to predict the failure of zircaloy-4 fuel sheathing during postulated local conditions”, *Journal of Nuclear Materials*, vol. 120, no. 1, pp. 41-54, 1984.
- [23] P. Wang, “Corrosion behaviour of zirconium alloys in high temperature aqueous environment by electrochemical impedance spectroscopy”, *Doctoral Dissertation, University of Manchester, Manchester*, 2011.
- [24] C.L. Whitmarsh, “Review of Zircaloy-2 and Zircaloy-4 properties relevant to NS Savannah reactor design”, *Oak Ridge National Laboratory*, no. ORNL-3281, 1962.
- [25] H.S. Rosenbaum, J. H. Davies, and J. Q. Pon, “Interaction of Iodine With Zircaloy-2”, No. GEAP--5100-5; EURAEC--1845, 1966.

- [26] R.D Page, “Canadian Power Reactor Fuel”, *Atomic Energy of Canada Limited*, no. AECL-5609, 1976.
- [27] D.G. Hardy, J.C. Wood, A.S. Bain, “CANDU Fuel Performance and Development”, *Atomic Energy of Canada Limited*, AECL-6213, *18th Annual International Conference of the Canadian Nuclear Association, Nuclear Fuels and Fuel Recycles Session*, Ottawa, 1978.
- [28] B. Cox, “Pellet-Clad Interaction (PCI) Failures of Zirconium Alloy Fuel Cladding—A Review”, *Journal of Nuclear Materials*, vol. 172, no. 3, pp. 249-29, 1990.
- [29] K. Une, “Stress Corrosion Cracking of Zircaloy-2 Cladding in Iodine Vapor”, *Journal of Nuclear Science and Technology*, vol. 14, no. 6, pp. 443-451, 1977.
- [30] P.S. Sidky, “Iodine stress corrosion cracking of zircaloy reactor cladding: iodine chemistry (a review)”, *Journal of Nuclear Materials*, vol. 256, no. 1, pp. 1-17, 1998.
- [31] D. Morgan, “A thermomechanical model of CANDU fuel”, *M.A.Sc. Thesis, Royal Military College of Canada*, Kingston, 2007.
- [32] F. Garzarolli, R. von Jan, H. Stehle, “The main causes of fuel element failure in water-cooled power reactors”, *Atomic Energy Review*, vol 17, no. 1, pp. 31-128, 1979.
- [33] M. Tayal, A.M. Manzer, R. Sejnoha, Y. Kinoshita, A.J. Hains, “The Integrity of CANDU Fuel during Load Following”, *The Tenth International Conference on Structural Mechanics in Reactor Technology*, Anaheim, 1989.
- [34] J.C. Wood, D.G. Hardy, A.S. Bain, “Improved CANDU Fuel Performance - A summary of previous AECL publications”, *Specialists' meeting on power ramping and power cycling of water reactor fuel and its significance to fuel behaviour*, Arles, France. 1979.
- [35] G.R. Fanjoy and A.S. Bain, “CANDU Fuel - Fifteen Years of Reactor Experience”, *International Conference on Nuclear Power and its Fuel Cycle*, International Atomic Energy Agency, Salzburg, 1977.
- [36] J.C. Wood, B.A. Surette, I. Atchison, “Pellet Cladding Interaction - Evaluation of Lubrication by Graphite”, *Journal of Nuclear Materials*, vol. 88, no. 1, pp. 81-94, 1980.
- [37] P.K. Chan and K.J. Kaddatz, “How does CANLUB work?”, *34<sup>th</sup> Annual Conference of the Canadian Nuclear Association*, Montreal, 1994.
- [38] G.A. Ferrier, J. Metzler, P.K. Chan, E.C. Corcoran, “Mitigating the Stress Corrosion Cracking of Zircaloy-4 Fuel Sheathing: Siloxane Coatings Revisited,” *Journal of Nuclear Engineering and Radiation Science*, vol. 2, no. 2, 2017.

- [39] M. Tayal, A. Sun, M. Gacesa, P. Reid, P. Fehrenbach, B. Surette, E. Suk, “Mechanism of power ramp failures in CANDU fuel”, *International Conference on CANDU Fuel*, Ottawa, 2008.
- [40] L. Fournier, A. Serres, Q. Auzoux, D. Leboulch, G.S. Was, “Proton irradiation effect on microstructure, strain localization and iodine-induced stress corrosion cracking in Zircaloy-4”, *Journal of Nuclear Materials*, vol. 384 no. 1, pp. 38-47, 2009.
- [41] Nuclear share figures, 2002-2012, *World Nuclear Association*, Available at: <http://www.world-nuclear.org/info/Facts-andFigures/Nuclear-generation-by-country>, 2013, Accessed on August 2, 2018.
- [42] 2017 Electricity Data, *Independent Electricity System Operator*, Available at: <http://ieso.ca/corporate-ieso/media/year-end-data>, Accessed on August 1, 2018.
- [43] The Canadian Nuclear Factbook, *Canadian Nuclear Association*, 2017, Available at: <https://cna.ca/wp-content/uploads/2017/01/2017-Factbook-EN-WEB-FINAL.pdf>, Accessed on August 7, 2018.
- [44] About Us, *Bruce Power*, Available at: <http://www.brucepower.com/about-us/>, Accessed on: August 2nd, 2018.
- [45] Regulated Price Plan, Price Report, May 1, 2017, to April 30, 2018, *Ontario Energy Board*, April 20, 2017, Available at: [https://www.oeb.ca/sites/default/files/rpp\\_price\\_report\\_20170420.pdf](https://www.oeb.ca/sites/default/files/rpp_price_report_20170420.pdf), pp.21, Accessed on: August 8, 2018.
- [46] About OPG, *Ontario Power Generation*, Available at: <https://www.opg.com/about/Pages/about.aspx>, Accessed on: August 2nd, 2018.
- [47] OPG Payment Amounts for Prescribed Generation Facilities, *Ontario Energy Board*, Available at: <https://www.oeb.ca/industry/applications-oeb/opg-payment-amounts-prescribed-generation-facilities>, Accessed on: August 1st, 2018.
- [48] Nuclear Contracting Toolkit, Glossary of Terms, *International Atomic Energy Agency*, Available at: <https://www.iaea.org/NuclearPower/Infrastructure/NuclearContractingToolkit/glossary.html>, Accessed on: July 31, 2018
- [49] Ontario Planning Outlook, A technical report on the electricity system prepared by the IESO, *Independent Electricity System Operator*, pp.12, September 1, 2016.
- [50] Darlington Refurbishment, *Ontario Power Generation*, Available at: <https://www.opg.com/darlington-refurbishment/Pages/default.aspx>, Accessed: July 31, 2018.
- [51] Life Extension Programs, *Bruce Power*, Available at: <http://www.brucepower.com/about-us/life-extension/>, Accessed on: July 31, 2018.

- [52] Ontario's Long-Term Energy Plan, *Government of Ontario, Ministry of Energy, Northern Development and Mines*, Available at: <https://www.ontario.ca/page/ontarios-long-term-energy-plan>, Accessed on: August 9, 2018.
- [53] M. Tayal, A. Ranger, N. Singhal, R. Mak, "Evolution of the ELESTRES Code for Applications to Extended Burnups", *Atomic Energy of Canada Limited, no. AECL-9947*, 1990.
- [54] M. Piro, D. Sunderland, W. Revie, S. Livingstone, I. Dimayuga, A. Douchant, M. Wright, "Potential mitigation strategies for preventing stress corrosion cracking failures in high-burnup CANDU fuel", *CNL Nuclear Review*, vol. 5, pp. 1-20, 2016.
- [55] M.R. Floyd, D.A. Leach, R.E. Moeller, R. R. Elder, R. J. Chenier, D. O'Brien, "Behaviour of Bruce NGS A fuel irradiated to a burnup of ~ 500 MWh/kgU," *Atomic Energy of Canada Limited, no. AECL--10685*, 1992.
- [56] A.D. Quastel, E.C. Corcoran, and B.J. Lewis, "The Effect of Oxidized UO<sub>2</sub> on Iodine-Induced Stress Corrosion Cracking of Fuel Sheathing", *12th International Conference on CANDU Fuel, Canadian Nuclear Society*, Kingston, 2013.
- [57] M. Farahani, G.A. Ferrier, P.K. Chan, E.C. Corcoran, "Beyond Canlub: An Improved Alternative Coating Development", *12th International Conference on CANDU Fuel, Canadian Nuclear Society*, Kingston, 2013.
- [58] J. Metzler, G.A. Ferrier, M. Farahani, P.K. Chan, E.C. Corcoran, "Investigating the Application of Alkali Metal Oxides and Alkaline Earth Metal Oxides as a Mitigation Strategy for Iodine-Induced Stress Corrosion Cracking in CANDU Fuel Sheathing", *35<sup>th</sup> Annual Conference of the Canadian Nuclear Society*, Saint John, 2015.
- [59] H.E. Rosinger and D.O. Northwood, "The elastic properties of zirconium alloy fuel cladding and pressure tubing materials", *Journal of Nuclear Materials*, vol. 79, no. 1, pp. 170-179, 1979.
- [60] I.A. Oding, V.S. Ivanova, V.V. Burdukskii, and V.N. Geminov, "Creep and stress relaxation in Metals", *Oliver and Boyd*, pp. 270-271, 1965.
- [61] T. J. Quirk, "One-way analysis of variance (ANOVA)", *Excel 2013 for Social Sciences Statistics*, pp. 177-196. Springer, Cham, 2015.
- [62] D.M. Diez, C.D. Barr, M. Cetinkaya-Rundel, "OpenIntro Statistics", *CreateSpace*, 2012.
- [63] J.M. Bland, D.G. Bland, "Statistics Notes: One and two sided tests of significance", *BMJ*, 309.6949, 1994.

- [64] F. Mosteller, and J.W. Tukey, “Data analysis and regression: a second course in statistics”, *Addison-Wesley Series in Behavioral Science: Quantitative Methods*, 1977.
- [65] A. Tasooji, R.E. Einziger, and A.K. Miller, “Modeling of zircaloy stress-corrosion cracking: texture effects and dry storage spent fuel behavior”, *Zirconium in the Nuclear Industry*, ASTM International, 1982.
- [66] M.A. Efrogmson, “Multiple Regression Analysis”, *Mathematical Methods for Digital Computers*, John Wiley & Sons, pp. 191-203, 1960.
- [67] Reactor Physics, “Science and Reactor Fundamentals – Reactor Physics”, *Canadian Nuclear Safety Commission*, Technical Training Group, Available at: <https://canteach.candu.org/Content%20Library/20030101.pdf>, Accessed on: August 14, 2018.
- [68] Reactor Physics, “Science and Reactor Fundamentals – Reactor Physics”, *Canadian Nuclear Safety Commission*, Technical Training Group, Available at: <https://canteach.candu.org/Content%20Library/20030101.pdf>, Accessed on: August 14, 2018.
- [69] M.A. Lone, “Nuclear Sources of Hydrogen in CANDU Fuel Channels,” *Atomic Energy of Canada Limited*, no. AECL-10630, 1998.
- [70] Neutron Activation and Scattering Calculation, *National Institute of Standards and Technology Center for Neutron Research*, Available at: <https://www.ncnr.nist.gov/resources/activation/>, Accessed on: August 14, 2018.
- [71] O.Y. Palazhchenko, “A Comprehensive CANDU-6 Model : Primary Side Transport of Dissolved and Particulate Radioactive Species, Doctoral Dissertation, University of New Brunswick, 2017.
- [72] P.V. Balakrishnan and G.M. Allison, “Some in loop experiments on corrosion product transport water chemistry,” *Nuclear Technology*, vol. 39, pp. 105119, 1978.
- [73] Deuterium Oxide, *Sigma-Aldrich*, Available at: <https://www.sigmaaldrich.com/catalog/product/aldrich/151882?lang=en&region=CA>, Accessed on: November 12, 2018.
- [74] K.A. Burrill, “An activity transport model for CANDU based on iron transport in the primary circuit,” *Atomic Energy of Canada Limit*, No. AECL-11805, 1998.

## 9 Appendix

### 9.1 Baseline Slotted Ring ANOVAs

#### ANOVA - 45 g Deflection Results

<i>Source of Variation</i>	<i>SS</i>	<i>df</i>	<i>MS</i>	<i>F</i>	<i>P-value</i>	<i>F crit</i>
Between Groups	0.01	2.00	0.00	1.96	0.22	5.14
Within Groups	0.01	6.00	0.00			
Total	0.01	8.00				

#### ANOVA - 95 g Deflection Results

<i>Source of Variation</i>	<i>SS</i>	<i>df</i>	<i>MS</i>	<i>F</i>	<i>P-value</i>	<i>F crit</i>
Between Groups	0.00	2.00	0.00	2.19	0.19	5.14
Within Groups	0.00	6.00	0.00			
Total	0.00	8.00				

#### ANOVA - Slot Size Results

<i>Source of Variation</i>	<i>SS</i>	<i>df</i>	<i>MS</i>	<i>F</i>	<i>P-value</i>	<i>F crit</i>
Between Groups	0.01	2.00	0.00	3.34	0.11	5.14
Within Groups	0.00	6.00	0.00			
Total	0.01	8.00				

### 9.2 Full Experimental Matrix

<b>Wedge Size / mm</b>	<b>Temperature / °C</b>	<b>Iodine / mg</b>	<b>O<sub>2</sub> Gas / Torr</b>	<b>Na<sub>2</sub>O / g</b>	<b>CaO / g</b>	<b>N</b>
N/A	N/A	0	0	0	0	9
4.5	300	0	0	0	0	4

6	300	0	0	0	0	4
7	300	0	0	0	0	4
9	300	0	0	0	0	8
12	300	0	0	0	0	4
6	375	0	0	0	0	4
7	375	0	0	0	0	4
9	375	0	0	0	0	4
12	375	0	0	0	0	4
4.5	300	255	0	0	0	4
6	300	255	0	0	0	4
7	300	255	0	0	0	4
9	300	255	0	0	0	8
12	300	255	0	0	0	3
6	375	255	0	0	0	4
7	375	255	0	0	0	4
6	300	1530	0	0	0	3
7	300	1530	0	0	0	4
9	300	1530	0	0	0	12
12	300	1530	0	0	0	4
9	375	1530	0	0	0	4
12	375	1530	0	0	0	4

6	300	1530	6	0	0	4
9	300	1530	6	0	0	8
12	300	1530	6	0	0	4
6	375	1530	6	0	0	4
7	375	1530	6	0	0	8
12	375	1530	6	0	0	3
9	300	1530	12	0	0	4
12	300	1530	12	0	0	4
9	375	1530	12	0	0	7
7	300	1530	54	0	0	4
9	300	1530	54	0	0	11
6	375	1530	54	0	0	4
9	375	1530	54	0	0	10
12	375	1530	54	0	0	4
6	300	1530	0	0.68	0	8
9	300	1530	0	0.68	0	4
12	300	1530	0	0.68	0	4
9	300	1530	0	0.84	0	8
6	300	1530	0	0	0.08	8
9	300	1530	0	0	0.08	8
12	300	1530	0	0	0.08	8

6	300	1530	0	0	0.17	8
9	300	1530	0	0	0.17	8
12	300	1530	0	0	0.17	8
6	300	1530	0	0	0.25	8
9	300	1530	0	0	0.25	8
12	300	1530	0	0	0.25	8
6	300	1530	0	0	0.33	8
9	300	1530	0	0	0.33	8
12	300	1530	0	0	0.33	8

### 9.3 Baseline Slotted Ring Deflection Results

Batch	Sample Number	45g Displacement / mm	95g Displacement / mm	Slot Size / mm
1	1	0.40	0.79	2.34
	2	0.48	0.83	2.26
	3	0.40	0.80	2.27
	<i>Average</i>	<i>0.42</i>	<i>0.80</i>	<i>2.29</i>
2	1	0.35	0.79	2.33
	2	0.35	0.76	2.35
	3	0.40	0.80	2.36
	<i>Average</i>	<i>0.37</i>	<i>0.78</i>	<i>2.35</i>
3	1	0.45	0.84	2.32
	2	0.40	0.82	2.30
	3	0.39	0.80	2.29
	<i>Average</i>	<i>0.41</i>	<i>0.82</i>	<i>2.30</i>
<b>Total</b>	<b><i>Average</i></b>	<b><i>0.40</i></b>	<b><i>0.80</i></b>	<b><i>2.31</i></b>
	<b><i>St.Dev</i></b>	<b><i>0.04</i></b>	<b><i>0.02</i></b>	<b><i>0.04</i></b>

### 9.4I-SCC Deflection Results

<b>Iodine / mg</b>	<b>Wedge Size / mm</b>	<b>Temperature / °C</b>	<b>45g Displacement / mm</b>	<b>95g Displacement / mm</b>	<b>Slot Size / mm</b>
0	4.5	300	0.351	0.818	2.81
0	4.5	300	0.4	0.775	2.76
0	4.5	300	0.402	0.823	2.77
0	4.5	300	0.386	0.795	2.93
0	6	300	0.405	0.92	3.76
0	6	300	0.423	0.915	3.73
0	6	300	0.455	0.861	3.75
0	6	300	0.432	0.905	3.69
0	7	300	0.432	0.876	4.63
0	7	300	0.447	0.982	4.52
0	7	300	0.438	0.901	4.58
0	7	300	0.449	0.918	4.57
0	9	300	0.441	0.959	6.7
0	9	300	0.471	0.946	6.72
0	9	300	0.432	0.969	6.6
0	9	300	0.49	0.939	6.65
0	9	300	0.41	0.867	5.87
0	9	300	0.398	0.851	5.89
0	9	300	0.391	0.838	5.84
0	9	300	0.421	0.838	6.12
0	12	300	0.397	0.862	9.6
0	12	300	0.479	0.913	9.65
0	12	300	0.415	0.841	9.6
0	12	300	0.436	0.859	9.68
0	6	375	0.414	0.893	4.99
0	6	375	0.451	0.89	5.04
0	6	375	0.443	0.93	5.01
0	6	375	0.438	0.879	4.97
0	7	375	0.478	0.957	5.95
0	7	375	0.448	0.951	5.9

0	7	375	0.452	0.953	5.88
0	7	375	0.47	0.969	5.9
0	9	375	0.477	0.981	7.78
0	9	375	0.465	0.938	7.82
0	9	375	0.452	0.955	7.79
0	9	375	0.433	0.902	7.72
0	12	375	0.41	0.82	10.74
0	12	375	0.43	0.83	10.8
0	12	375	0.47	0.93	10.84
0	12	375	0.42	0.86	10.72
255	4.5	300	0.422	0.795	2.67
255	4.5	300	0.393	0.845	2.71
255	4.5	300	0.396	0.802	2.64
255	4.5	300	0.377	0.851	2.73
255	6	300	0.4	0.854	3.57
255	6	300	0.406	0.853	3.54
255	6	300	0.445	0.832	3.58
255	6	300	0.386	0.852	3.55
255	7	300	0.4	0.849	4.29
255	7	300	0.406	0.867	4.23
255	7	300	0.445	0.894	4.13
255	7	300	0.386	0.839	4.16
255	9	300	0.448	1.059	6.57
255	9	300	0.455	0.959	6.51
255	9	300	0.461	0.92	6.48
255	9	300	0.432	0.94	6.42
255	9	300	0.446	0.908	5.8
255	9	300	0.468	0.9	5.82
255	9	300	0.444	0.894	5.84
255	9	300	0.499	0.956	5.77
255	12	300	0.454	0.956	9.41
255	12	300	0.484	0.921	9.37
255	12	300	0.455	0.925	9.44
255	6	375	0.421	0.932	4.92

255	6	375	0.442	0.893	5.04
255	6	375	0.484	0.946	5.1
255	6	375	0.441	1.002	5.09
255	7	375	0.455	0.946	5.89
255	7	375	0.479	0.994	5.89
255	7	375	0.452	0.947	5.94
255	7	375	0.458	0.961	5.96
1530	6	300	0.483	0.998	4.64
1530	6	300	0.485	0.96	4.6
1530	6	300	0.478	1.001	4.67
1530	6	300	0.531	1.288	4.53
1530	7	300	0.533	1.098	3.6
1530	7	300	0.498	0.939	3.75
1530	7	300	0.501	1.063	3.81
1530	7	300	0.496	0.932	3.76
1530	9	300	0.514	1.084	6.87
1530	9	300	0.484	1.221	6.69
1530	9	300	0.657	1.327	6.41
1530	9	300	0.528	1.11	6.71
1530	9	300	0.508	1.228	6.75
1530	9	300	0.536	1.038	6.64
1530	9	300	0.561	1.122	6.52
1530	9	300	0.544	1.154	6.54
1530	9	300	0.471	0.983	5.97
1530	9	300	0.466	0.966	5.93
1530	9	300	0.599	0.975	6.17
1530	9	300	0.478	1.221	5.84
1530	12	300	0.471	0.966	8.84
1530	12	300	0.466	0.971	8.74
1530	12	300	0.599	1.25	8.87
1530	12	300	0.478	0.962	8.91
1530	9	375	0.602	1.251	8.98
1530	9	375	0.642	1.347	9.01
1530	9	375	0.639	1.304	9.05

1530	9	375	0.568	1.175	8.95
1530	12	375	0.44	0.93	12
1530	12	375	0.45	0.95	11.95
1530	12	375	0.44	0.88	11.92
1530	12	375	0.59	1.14	12.2

### 9.5 O<sub>2</sub> Gas Deflection and Slot Size Results

<b>Iodine / mg</b>	<b>Wedge Size / mm</b>	<b>Temperature / °C</b>	<b>O<sub>2</sub> gas / Torr</b>	<b>45g Displacement / mm</b>	<b>95g Displacement / mm</b>	<b>Slot Size / mm</b>
1530	9	300	54	0.517	1.06	6.5
1530	9	300	54	0.497	1.08	5.62
1530	9	300	54	0.478	0.984	6.02
1530	9	300	54	0.471	1.024	5.9
1530	7	300	54	0.499	1.003	4.2
1530	7	300	54	0.558	1.102	4.95
1530	7	300	54	0.441	0.945	4.22
1530	7	300	54	0.513	1.063	4.6
1530	9	300	54	0.451	0.923	5.93
1530	9	300	54	0.453	0.909	5.54
1530	9	300	54	0.448	0.985	5.7
1530	9	300	54	0.498	1.004	5.49
1530	9	300	54	0.497	1.0063	5.87
1530	9	300	54	0.435	0.914	5.49
1530	9	300	54	0.489	0.977	5.78
1530	9	300	54	0.716	1.446	7.4
1530	9	375	54	0.488	1.053	8.85
1530	9	375	54	0.483	1.009	8.49
1530	9	375	54	0.584	1.159	8.94
1530	9	375	54	0.547	1.074	8.95
1530	9	375	54	0.531	1.062	8.96
1530	9	375	54	0.549	1.11	8.93
1530	9	375	54	0.507	1.047	8.94
1530	9	375	54	0.489	0.996	8.51

1530	9	375	54	0.485	1.01	8.77
1530	9	375	54	0.502	1.083	8.99
1530	12	375	54	0.426	0.892	11.26
1530	12	375	54	0.447	0.961	11.97
1530	12	375	54	0.423	0.908	10.95
1530	12	375	54	0.444	0.999	11.76
1530	6	375	54	0.532	1.045	5.52
1530	6	375	54	0.549	1.041	5.64
1530	6	375	54	0.477	0.99	5.39
1530	6	375	54	0.552	0.957	5.45
1530	12	300	12	0.493	0.976	8.35
1530	12	300	12	0.488	1.017	8.5
1530	12	300	12	0.43	1.121	7.62
1530	12	300	12	0.444	0.963	8.8
1530	9	300	12	0.544	1.102	6.2
1530	9	300	12	0.478	1.031	5.37
1530	9	300	12	0.515	1.125	5.73
1530	9	300	12	0.489	1.043	5.5
1530	9	375	12	0.466	0.987	7.53
1530	9	375	12	0.498	0.977	7.72
1530	9	375	12	0.688	1.387	8.89
1530	9	375	12	0.682	1.374	8.94
1530	9	375	12	0.473	0.919	7.64
1530	9	375	12	0.453	0.901	7.52
1530	9	375	12	0.532	1.091	8.95
1530	9	375	12	0.545	1.143	8.83
1530	9	375	12	0.442	0.94	7.6
1530	9	375	12	0.646	1.308	8.93
1530	9	300	6	0.511	1.08	5.55
1530	9	300	6	0.506	1.005	5.4
1530	9	300	6	0.449	0.929	5.6
1530	9	300	6	0.51	0.965	5.6
1530	9	300	6	0.452	0.975	5.62
1530	9	300	6	0.46	0.982	5.63

1530	9	300	6	0.499	1.031	5.48
1530	9	300	6	0.471	0.967	5.61
1530	6	300	6	0.472	0.954	3.4
1530	6	300	6	0.469	0.989	3.4
1530	6	300	6	0.445	0.967	3.5
1530	6	300	6	0.499	1.045	3.45
1530	12	300	6	0.478	0.999	8.45
1530	12	300	6	0.479	0.989	8.48
1530	12	300	6	0.474	1.039	8.36
1530	12	300	6	0.538	1.109	7.84
1530	12	375	6	0.426	0.933	11.87
1530	12	375	6	0.506	0.904	11.95
1530	12	375	6	0.615	1.359	12.06
1530	12	375	6	0.498	0.856	11.69
1530	7	375	6	0.479	0.939	5.94
1530	7	375	6	0.484	0.955	5.92
1530	7	375	6	0.538	1.162	6.95
1530	7	375	6	0.472	0.986	6.28
1530	6	375	6	0.521	1.027	5.89
1530	6	375	6	0.563	1.188	5.95
1530	6	375	6	0.628	1.379	5.97
1530	6	375	6	0.625	1.179	6.01
1530	7	375	6	0.445	1.017	6.29
1530	7	375	6	0.533	0.974	6.58
1530	7	375	6	0.425	0.967	6.35
1530	7	375	6	0.436	0.905	5.71

### 9.6 Oxide Additive Deflection and Slot Size Results

Iodine / mg	Wedge Size / mm	Temperature / °C	Na <sub>2</sub> O / g	CaO / g	45g Displacement / mm	95g Displacement / mm	Slot Size / mm
1530	9	300	0.84	0	0.428	0.891	5.51
1530	9	300	0.84	0	0.427	0.882	5.52
1530	9	300	0.84	0	0.457	0.932	5.37

1530	9	300	0.84	0	0.412	0.863	5.56
1530	9	300	0.84	0	0.4	0.83	8.43
1530	9	300	0.84	0	0.405	0.855	8.11
1530	9	300	0.84	0	0.402	0.83	8.13
1530	9	300	0.84	0	0.404	0.859	8.12
1530	12	300	0.68	0	0.473	0.904	8.56
1530	12	300	0.68	0	0.449	0.933	8.73
1530	12	300	0.68	0	0.459	0.913	8.51
1530	12	300	0.68	0	0.463	0.936	8.45
1530	9	300	0.68	0	0.449	0.91	5.71
1530	9	300	0.68	0	0.431	0.882	5.85
1530	9	300	0.68	0	0.445	0.873	5.78
1530	9	300	0.68	0	0.419	0.865	5.92
1530	6	300	0.68	0	0.548	1.077	4.61
1530	6	300	0.68	0	0.502	1.071	4.55
1530	6	300	0.68	0	0.577	1.082	4.62
1530	6	300	0.68	0	0.536	1.034	4.34
1530	6	300	0.68	0	0.546	1.031	4.54
1530	6	300	0.68	0	0.504	0.998	4.36
1530	6	300	0.68	0	0.495	0.985	4.35
1530	6	300	0.68	0	0.593	1.152	4.58
1530	6	300	0	0.33	0.399	0.824	4.59
1530	6	300	0	0.33	0.375	0.809	3.95
1530	6	300	0	0.33	0.431	0.823	3.96
1530	6	300	0	0.33	0.415	0.835	4.01
1530	6	300	0	0.33	0.403	0.858	3.93
1530	6	300	0	0.33	0.428	0.865	4.01
1530	6	300	0	0.33	0.42	0.862	3.92
1530	6	300	0	0.33	0.403	0.858	4.11
1530	12	300	0	0.33	0.429	0.863	8.94
1530	12	300	0	0.33	0.407	0.808	9.16
1530	12	300	0	0.33	0.399	0.823	8.96
1530	12	300	0	0.33	0.468	0.843	8.96
1530	12	300	0	0.33	0.404	0.843	8.82

1530	12	300	0	0.33	0.413	0.816	8.96
1530	12	300	0	0.33	0.425	0.837	9.26
1530	12	300	0	0.33	0.391	0.79	8.74
1530	9	300	0	0.33	0.434	0.819	5.89
1530	9	300	0	0.33	0.453	0.898	5.99
1530	9	300	0	0.33	0.418	0.855	6.44
1530	9	300	0	0.33	0.402	0.83	6.07
1530	9	300	0	0.335	0.41	0.859	6.08
1530	9	300	0	0.33	0.389	0.812	5.96
1530	9	300	0	0.33	0.431	0.862	6.34
1530	9	300	0	0.33	0.416	0.894	6.13
1530	6	300	0	0.17	0.479	0.867	4.01
1530	6	300	0	0.17	0.514	0.868	4.1
1530	6	300	0	0.17	0.41	0.856	4.12
1530	6	300	0	0.17	0.452	0.824	4.51
1530	6	300	0	0.17	0.502	0.887	4.89
1530	6	300	0	0.17	0.446	0.899	4.11
1530	6	300	0	0.17	0.427	0.842	4.11
1530	6	300	0	0.17	0.521	0.856	4.12
1530	9	300	0	0.17	0.439	0.937	6.5
1530	9	300	0	0.17	0.431	0.883	6.54
1530	9	300	0	0.17	0.422	0.858	6.4
1530	9	300	0	0.17	0.417	0.879	6.57
1530	9	300	0	0.17	0.442	0.877	6.66
1530	9	300	0	0.17	0.423	0.895	6.94
1530	9	300	0	0.17	0.42	0.847	6.93
1530	9	300	0	0.17	0.403	0.835	6.88
1530	12	300	0	0.17	0.472	1.025	8.59
1530	12	300	0	0.17	0.503	1.02	8.3
1530	12	300	0	0.17	0.498	0.987	8.62
1530	12	300	0	0.17	0.488	0.983	8.49
1530	12	300	0	0.17	0.53	0.985	8.72
1530	12	300	0	0.17	0.49	1	8.49
1530	12	300	0	0.17	0.494	0.984	8.5

1530	12	300	0	0.17	0.449	0.912	8.48
1530	9	300	0	0.08	0.542	1.171	7.2
1530	9	300	0	0.08	0.523	1.052	7.15
1530	9	300	0	0.08	0.524	1.052	7.05
1530	9	300	0	0.08	0.525	1.048	7.3
1530	9	300	0	0.08	0.543	1.093	7.37
1530	9	300	0	0.08	0.616	1.289	6.84
1530	9	300	0	0.08	0.515	1.032	7.33
1530	9	300	0	0.08	0.505	1.037	7.22
1530	12	300	0	0.08	0.501	1.039	10.08
1530	12	300	0	0.08	0.567	1.17	10.28
1530	12	300	0	0.08	0.488	1.029	10.1
1530	12	300	0	0.08	0.543	1.126	10.08
1530	12	300	0	0.08	0.488	1.04	10.13
1530	12	300	0	0.08	0.513	1.016	10.16
1530	12	300	0	0.08	0.548	1.067	10
1530	12	300	0	0.08	0.502	1.04	10.23
1530	6	300	0	0.08	0.565	1.125	4.6
1530	6	300	0	0.08	0.568	1.045	4.5
1530	6	300	0	0.08	0.559	1.045	4.56
1530	6	300	0	0.08	0.539	1.144	4.57
1530	6	300	0	0.08	0.542	1.167	4.47
1530	6	300	0	0.08	0.543	1.166	4.52
1530	6	300	0	0.08	0.578	1.124	4.51
1530	6	300	0	0.08	0.559	1.06	4.6